

scientific data



OPEN

DATA DESCRIPTOR

EarSet: A Multi-Modal Dataset for Studying the Impact of Head and Facial Movements on In-Ear PPG Signals

Alessandro Montanari^{1,4}✉, Andrea Ferlini^{1,2,4}✉, Ananta Narayanan Balaji³, Cecilia Mascolo² & Fahim Kawzar¹

Photoplethysmography (PPG) is a simple, yet powerful technique to study blood volume changes by measuring light intensity variations. However, PPG is severely affected by motion artifacts, which hinder its trustworthiness. This problem is pressing in earables since head movements and facial expressions cause skin and tissue displacements around and inside the ear. Understanding such artifacts is fundamental to the success of earables for accurate cardiovascular health monitoring. However, the lack of in-ear PPG datasets prevents the research community from tackling this challenge. In this work, we report on the design of an ear tip featuring a 3-channels PPG and a co-located 6-axis motion sensor. This, enables sensing PPG data at multiple wavelengths and the corresponding motion signature from both ears. Leveraging our device, we collected a multi-modal dataset from 30 participants while performing 16 natural motions, including both head/face and full body movements. This unique dataset will greatly support research towards making in-ear vital signs sensing more accurate and robust, thus unlocking the full potential of the next-generation PPG-equipped earables.

Background & Summary

Monitoring vital signs, such as cardiovascular functions, heart rate, oxygen saturation, and blood pressure, through Photoplethysmography (PPG) is common across wearables like smartwatches¹. Photoplethysmography, as suggested by its name, is an optical technique used to infer blood volumetric changes in the peripheral circulation. PPG is indeed a remarkable signal, which not only carries a wealth of clinical information (such as heart rate, heart rate variability, blood oxygen saturation, respiration rate, blood pressure, and artery characteristics²⁻⁴), but can also be used for non-medical applications such as authentication⁵ and drowsiness detection⁶.

At the same time, the past years have witnessed the widespread diffusion of a new family of wearables: smart earbuds (also known as *earables*). Earables are mostly known for their leisure applications (e.g., Apple AirPods), showing their capability in enhancing the user's auditory experience with, for instance, noise cancellation and spatially aware audio. However, they are also gaining traction, across the research community, for personal health monitoring⁷⁻¹⁰, activity recognition¹¹⁻¹⁴, authentication¹⁵, and navigation¹⁶. Earables are poised to revolutionize the mobile health (*mHealth*) market¹⁷. Thanks to their proximity to the human sensorium (i.e., brain, ears, eyes, mouth, and nose), earables are in a unique position with respect to other, more traditional, wearables like smartwatches¹⁸. Indeed, earables have allowed the research community to investigate a number of novel applications such as monitoring cerebral activity during sleep through electroencephalography (EEG)¹⁹, eye-movements²⁰ and tracking eating episodes, dietary and swallowing activities²¹.

Notably, previous works have explored PPG sensing in or around the ear focusing on specific applications. However, PPG signal acquisition is particularly challenging in the presence of either ambient light or motion. While the former can be mitigated by ambient light rejection modules (often already implemented in hardware), there still is no unanimously agreed technique to mitigate the latter without a considerable loss of information. Earlier works considered only motion artifacts (MA) arising from body movements, like walking or

¹Nokia Bell Labs, Cambridge, UK. ²University of Cambridge, Cambridge, UK. ³National University of Singapore, Singapore, Singapore. ⁴These authors contributed equally: Alessandro Montanari, Andrea Ferlini. ✉e-mail: alessandro.montanari@nokia-bell-labs.com; andrea.ferlini@nokia-bell-labs.com



oPeN

日期 Descriptor

EarSet：用于研究头部和面部运动对耳内PPG信号影响的多模态数据集

亚历山德罗·蒙塔纳里[✉]，安德里亚·费里尼[✉]、阿南塔·纳拉亚南·巴拉吉、塞西莉亚·马斯科洛
&法希姆·考萨尔

光电容积描记术（PPG）是一种简单但功能强大的技术，通过测量光强度变化来研究血容量变化。然而，PPG受到运动伪影的严重影响，这阻碍了其可信度。这个问题是紧迫的，因为头部运动和面部

表情会导致耳朵周围和内部的皮肤和组织移位。了解这些文物是可穿戴设备成功进行准确心血管健康监测的基础。然而，由于缺乏耳内PPG数据集，研究界无法应对这一挑战。在这项工作中，我们报告了一个具有3通道PPG和一个共同定位的6轴运动传感器的耳塞的设计。这使得能够感测多个波长处的PPG数据和来自双耳的对应运动特征。利用我们的设备，我们从30名参与者中收集了一个多模态数据集，同时执行16个自然运动，包括头部/面部和全身运动。这个独特的数据集将极大地支持研究，使入耳式生命体征传感更加准确和强大，从而释放下一代配备PPG的可穿戴设备的全部潜力。

背景和摘要

通过光电容积描记术（PPG）监测生命体征，如心血管功能、心率、血氧饱和度和血压，在智能手表等可穿戴设备中很常见。光电容积描记术，顾名思义，是一种用于推断外周循环中血液体积变化的光学技术。PPG确实是一个了不起的信号，它不仅携带了丰富的临床信息（如心率、心率变异性、血氧饱和度、呼吸率、血压和动脉特征），而且还可以用于非医疗应用，如身份验证和嗜睡检测。

与此同时，过去几年见证了一个新的可穿戴设备家族的广泛传播：智能耳塞（也称为earables）。可穿戴设备主要以其休闲应用而闻名（例如，Apple AirPods），展示了它们在增强用户听觉体验方面的能力，例如噪音消除和空间感知音频。然而，在整个研究界，它们也在个人健康监测、活动识别、身份验证和导航方面获得了越来越多的关注。可穿戴设备将彻底改变移动的健康（mHealth）市场。由于它们接近人类的感觉中枢（即，大脑、耳朵、眼睛、嘴巴和鼻子），相对于其他更传统的可穿戴设备（如智能手表），可穿戴设备处于独特的地位。事实上，可穿戴设备已经使研究界能够研究许多新的应用，例如通过脑电图（EEG）监测睡眠期间的大脑活动，眼球运动以及跟踪进食事件，饮食和吞咽活动。

值得注意的是，先前的工作已经探索了专注于特定应用的耳朵中或周围的PPG感测。然而，PPG信号采集在存在环境光或运动的情况下尤其具有挑战性。虽然前者可以通过环境光抑制模块（通常已经在硬件中实现）来减轻，但仍然没有一致同意的技术来减轻后者而不会造成相当大的信息损失。早期的作品只考虑了由身体运动引起的运动伪影（MA），如步行或

¹ nokia Bell Labs，坎布里奇，英国剑桥大学（University of Cambridge），剑桥，英国新加坡国立大学National University of Singapore，Singapore these authors contributed equally：Alessandro Montanari，Andrea Ferlini。电子邮件：alessandro.montanari@nokia-bell-labs.com 作者：Ferlini@nokia-bell-labs.com

Datasets	PPG sensor location	Motion being studied	Additional sensor data	Number of participants
Activity monitoring ⁴⁴	Wrist	Squat exercises, stepper exercises, and resting	3-channels PPG	7
			3-axis accelerometer	
PPG DaLiA ⁴⁵	Wrist	Daily life activities like sitting, walking, cycling, driving, working, etc.	3-channels PPG	15
			Electrocardiogram (ECG)	
			Electrodermal activity (EDA)	
			3-axis accelerometer	
			Respiration rate	
			Body temperature	
Effect of exercises on PPG signals ⁴⁶	Wrist	Walking, running, and biking	3-channels PPG	23
			Chest ECG	
			3-axis accelerometer	
			3-axis low noise accelerometer	
			3-axis gyroscope	
Motion artifact removal in PPG signals (IEEE signal processing cup) ⁴⁷	Wrist	Random physical exercises without labels	3-channels PPG	12 (training dataset) 10 (test dataset)
			Chest ECG	
			3-axis accelerometer	
Motion artifact cancellation ⁴⁸	Wrist	Walking and running	3-channels PPG	24
			Chest ECG	
			3-axis accelerometer	
			3-axis gyroscope	
WESAD (Stress detection) ⁴⁹	Wrist and Chest	Intense physical activity and mental exercises to induce stress	Wrist PPG	17
			Wrist accelerometer	
			Wrist electrodermal activity (EDA)	
			Body temperarture	
			Chest ECG	
			Chest accelerometer	
			Chest EMG	
			Chest Respiration	
BIDMC dataset ⁵⁰	Finger	No exercise involved	Finger PPG	53
			Pneumography (Respiration)	
FatigueSet ²⁶	In-Ear	Running on a treadmill to induce physical fatigue	In-Ear PPG	12
			In-Ear IMU sensor	
			Chest ECG	
			Chest Respiration sensor	
			Wrist PPG	
			Wrist EDA	
			Wrist IMU	
Motion tolerant heart rate and Blood pressure monitoring ²⁷	Outside ear	Exercising on a bike	Body temperature sensor	14
			Ear PPG	
			Ear ECG	
EarSet	Stereo In-ear	16 different facial and head motions	Ambulatory blood pressure monitor	30
			In-Ear PPG (Both Left and right)	
			In-Ear IMU (Both Left and right)	
			Chest band ECG	
			Chest band Respiration sensor	

Table 1. PPG datasets publicly available for motion artifact studies.

running^{22–25}. However, the head and facial region consist of an intricate mesh of muscles and blood vessels that contract and relax with each of their movements. This induces unwanted noise and motion artifacts in the PPG signals recorded from the ear. The interaction between these motions and the signals recorded from in-ear PPG sensors remains entirely unexplored.

Very few openly available datasets feature PPG data from the ear^{26,27}. However, there are no publicly available datasets that explore the effect of facial expressions and head movements on earables. Table 1 presents an overview of existing datasets in the literature that provide PPG signals collected at various body locations. Recently²⁷, proposed a solution for how motion artifacts can be removed for accurate heart rate and blood pressure estimation with PPG sensors placed on the ear lobes. However, they only study the effect of body motion artifacts on

数据集	PPG传感器位置	正在研究的运动	附加传感器数据	数量 参与者
活动监视	手腕	深蹲练习、踏步机锻炼和休息	3-通道PPG 3-轴加速度计	7
PPG DaLiA	手腕	日常生活活动，如坐着、走路、骑自行车、驾驶、工作等。	3-通道PPG 心电图 (ECG) 皮肤电活动 (EDA) 3-轴加速度计 呼吸速率 体温	15
运动对PPG信号的影响	手腕	走路、跑步、自行车	3-通道PPG 胸部心电图 3-轴加速度计 3-轴向低噪声加速度计 3-轴陀螺仪	23
PPG信号中的运动伪影去除 (IEEE信号处理杯)	手腕	随机物理无标签练习	3-通道PPG 胸部心电图 3-轴加速度计	12 (培训) 数据集) 10 (test数据集)
运动伪影消除	手腕	步行和跑步	3-通道PPG 胸部心电图 3-轴加速度计 3-轴陀螺仪	24
WESAD (应力检测)	手腕和胸部	剧烈运动和心理练习，引起应力	腕部PPG 腕部加速度计 腕部皮肤电活动 (EDA) 体温 胸部心电图 胸部加速计 胸部肌电图 胸部呼吸	17
BIDMC数据集	手指	不涉及运动	手指PPG 呼吸描记术 (呼吸)	53
埃格塞特	入耳式	在跑步机上跑步，诱发体力疲劳	耳内PPG 入耳式IMU传感器 胸部心电图 胸部呼吸传感器 腕部PPG 腕部EDA 手腕IMU 体温传感器	12
运动耐受心率和血压监测	外耳	在自行车上锻炼	耳PPG 耳ECG 动态血压监测	14
EarSet	立体声入耳式	16种不同的面部和头部运动	耳内PPG (左侧和右侧) 入耳式IMU (左右) 胸带心电图 胸带呼吸传感器	30

表1. PPG数据集可公开用于运动伪影研究。

运行。然而，头部和面部区域由肌肉和血管组成的复杂网络组成，这些肌肉和血管随着它们的每次运动而收缩和放松。这在从耳朵记录的PPG信号中引起不必要的噪声和运动伪影。这些运动与从耳内PPG传感器记录的信号之间的相互作用仍然完全未被探索。

很少有公开可用的数据集具有来自耳朵的PPG数据。然而，目前还没有公开的数据集来探索面部表情和头部运动对可穿戴设备的影响。表1概述了文献中现有的数据集，这些数据集提供了在不同身体位置收集的PPG信号。最近，提出了一种解决方案，用于如何通过放置在耳垂上的PPG传感器消除运动伪影，以进行准确的心率和血压估计。然而，他们只研究了身体运动伪影对

the acquired PPG signals. Hence, there is a strong need for an open-source dataset studying the effect of facial motions on in-ear PPG signals.

To this end, this work aims at *providing the research community with a novel, multi-modal, dataset, which, for the first time, will allow studying of the impact of body and head/face movements on both the morphology of the PPG wave captured at the ear, as well as on the vital signs estimation*. To accurately collect in-ear PPG data, coupled with a 6 degrees-of-freedom (DoF) motion signature, we prototyped and built a flexible research platform for in-the-ear data collection. The platform is centered around a novel ear-tip design which includes a 3-channels PPG (green, red, infrared) and a 6-axis (accelerometer, gyroscope) motion sensor (IMU) co-located on the same ear-tip. This allows the simultaneous collection of spatially distant (i.e., one tip in the left and one in the right ear) PPG data at multiple wavelengths and the corresponding motion signature, for a total of 18 data streams. Inspired by the Facial Action Coding Systems (FACS)²⁸, we consider a set of potential sources of motion artifact (MA) caused by natural facial and head movements. Specifically, we gather data on 16 different head and facial motions, including head movements (nodding, shaking, tilting), eyes movements (vertical eyes movements, horizontal eyes movements, brow raiser, brow lowerer, right eye wink, left eye wink), and mouth movements (lip puller, chin raiser, mouth stretch, speaking, chewing). We also collect motion and PPG data under activities of different intensities, which entail the movement of the entire body (walking and running). Together with in-ear PPG and IMU data, we collect several other vital signs such as heart rate, heart rate variability, and breathing rate from a medical-grade chest device.

With approximately 17 hours of data from 30 participants of mixed gender and ethnicity (mean age: 28.7 years, standard deviation: 5.3 years), our dataset empowers the research community to analyze the morphological characteristics of in-ear PPG signals with respect to **motion, device positioning** (left ear, right ear), as well as a set of **configuration parameters** and their corresponding data quality/power consumption trade-off. We envision such a dataset could open the door to innovative filtering techniques to mitigate, and eventually eliminate, the impact of MA on in-ear PPG. We ran a set of preliminary analyses on the data and observe statistically significant morphological differences in the PPG signal across different types of motions when compared to a situation where there is no motion. These preliminary results represent the first step towards the detection of corrupted PPG segments and show the importance of studying how head/face movements impact PPG signals in the ear.

To the best of our knowledge, this is the first in-ear PPG dataset that covers a wide range of full-body and head/facial motion artifacts. Being able to study the signal quality and motion artifacts under such circumstances will serve as a reference for future research in the field, acting as a stepping stone to fully enable PPG-equipped earables.

Methods

To accurately analyze the in-ear PPG motion artifacts arising from head and facial motions, we design a controlled experiment and ask participants to perform a set of pre-defined body, head, and facial motions. We opted for a controlled study since it enables running a detailed analysis of the phenomenon under investigation and it is suitable for the reproducibility of the data collection procedure. In this section, we provide details regarding the study population, data collection procedure, and the collected data.

Participants. Thirty individuals (18 males, 12 females, 20–49 years of age, mean age: 28.7 years, standard deviation: 5.3 years) were recruited and voluntarily took part in the study. None of the participants had any underlying heart or respiratory condition and were in good health at the time of the study. We used the standard Fitzpatrick skin tone scale²⁹ to group our participants based on skin tone. The scale includes 6 types, 1 being the lightest and 6 being the darkest. Despite being dominated by type 2 skin tone ($n=18$), our dataset includes type 1 ($n=2$), type 3 ($n=4$), type 4 ($n=4$), and type 5 ($n=2$) skin tone groups.

Before taking part in the study, the investigators briefed all the participants who then gave their written consent (by completing an informed consent form) to release their data publicly. Every participant received a gift card as compensation upon completion of the study. The study was approved by the ethics board of the department of Computer Science and Technology at the University of Cambridge (application number 1873).

Devices and setup. Given the lack of existing open-source in-ear PPG platforms, we designed a custom head-worn prototype (see Fig. 1c) to collect in-ear PPG signals with established and affordable hardware components. The prototype consists of an ESP32 microcontroller collecting sensor data from both the left and right ears. In order to facilitate the PPG signal acquisition from inside the ear (Fig. 2), we fabricated a flexible PCB board consisting of a MAXM86161 (<https://www.maximintegrated.com/en/products/sensors/MAXM86161.html>) PPG sensor and ST-LSM6DSRX (<https://www.st.com/en/mems-and-sensors/lsm6dsrx.html>) IMU as shown in Fig. 1a. The flexible PCB board is interfaced via the I2C protocol to the ESP32 microcontroller for data acquisition. MAXM86161 is a well-known 3-channels PPG sensor (green - 520 to 550 nm, red - 660 nm, infrared - 880 nm) catered for in-ear sensing applications. The IMU continuously records 3-axis accelerometer and 3-axis gyroscope data to provide motion signals for in-ear motions occurring while making facial expressions or head movements. Both sensors are sampled at a frequency of 100 Hz. As shown in Fig. 1b, the flexible PCB containing the PPG sensor and the IMU was coated with soft silicone to resemble a typical ear tip to provide comfort while wearing the device, as well as remain firm within the ear during various face/head motions. We used a transparent soft silicone gel to prevent any distortions in the acquired PPG signals. Figure 2 reports a drawing of the device when placed inside the ear canal.

PPG signal quality is not only affected by motion but also by the sensor's configuration. Typically, sensors allow changing several parameters which affect the acquired signal and consequently the power consumed by the sensor. Given this trade-off, often, optimal parameters for signal quality are not the most efficient in terms

获取的PPG信号。因此，非常需要一个开源数据集来研究面部运动对耳内PPG信号的影响。

为此，这项工作旨在为研究界提供一种新颖的多模态数据集，该数据集将首次允许研究身体和头部/面部运动对在耳朵处捕获的PPG波的形态以及生命体征估计的影响。为了准确地收集耳内PPG数据，再加上6自由度（DoF）运动签名，我们原型设计并构建了一个用于耳内数据收集的灵活研究平台。该平台以一种新颖的耳塞设计为中心，包括一个3通道PPG（绿色、红色、红外）和一个6轴（加速度计、陀螺仪）运动传感器（IMU），共同位于同一个耳塞上。这允许同时收集空间上远离的（即，一个尖端在左耳，一个在右耳）多个波长的PPG数据和相应的运动特征，总共18个数据流。受面部动作编码系统（FACS）的启发，我们考虑了一组由自然面部和头部运动引起的运动伪影（MA）的潜在来源。具体来说，我们收集了16种不同的头部和面部运动的数据，包括头部运动（点头、摇晃、倾斜），眼睛运动（垂直眼睛运动，水平眼睛运动，眉毛抬起，眉毛降低，右眼眨眼，左眼眨眼）和嘴巴运动（嘴唇拉，下巴抬起，嘴巴伸展，说话，咀嚼）。我们还收集不同强度活动下的运动和PPG数据，这些活动需要整个身体的运动（步行和跑步）。与耳内PPG和IMU数据一起，我们从医疗级胸部设备收集其他几个生命体征，如心率、心率变异性和平吸率。

来自30名混合性别和种族的参与者的约17小时的数据（平均年龄：28.7岁，标准差：5.3年），我们的数据集使研究界能够分析耳内PPG信号与运动、设备定位（左耳、右耳）以及一组配置参数及其对应的数据质量/功耗权衡。我们设想这样的数据集可以为创新的滤波技术打开大门，以减轻并最终消除MA对耳内PPG的影响。我们对数据进行了一组初步分析，并观察到与没有运动的情况相比，不同类型运动的PPG信号存在统计学显著的形态差异。这些初步结果代表了检测受损PPG片段的第一步，并显示了研究头部/面部运动如何影响耳中PPG信号的重要性。

据我们所知，这是第一个耳内PPG数据集，涵盖了广泛的全身和头部/面部运动伪影。能够在这种情况下研究信号质量和运动伪影将作为该领域未来研究的参考，作为完全启用配备PPG的耳机的垫脚石。

方法

为了准确地分析由头部和面部运动引起的耳内PPG运动伪影，我们设计了一个受控实验，并要求参与者执行一组预定义的身体、头部和面部运动。我们选择了对照研究，因为它可以对研究中的现象进行详细分析，并且适合数据收集程序的重现性。在本节中，我们提供了有关研究人群、数据收集程序和收集的数据的详细信息。

参与者 招募了30名个体（18名男性，12名女性，20-49岁，平均年龄：28.7岁，标准差：5.3岁）并自愿参加研究。所有参与者都没有任何潜在的心脏或呼吸系统疾病，并且在研究时健康状况良好。我们使用标准的菲茨帕特里克肤色量表根据肤色对参与者进行分组。该量表包括6种类型，1为最轻，6为最暗。尽管以2型肤色（n=18）为主，但我们的数据集包括1型（n=2）、3型（n=4）、4型（n=4）和5型（n=2）肤色组。

在参与研究之前，研究人员向所有参与者简要介绍了他们的书面同意（通过填写知情同意书）公开发布他们的数据。每个参与者在完成研究后都会收到一张礼品卡作为补偿。这项研究得到了剑桥大学计算机科学与技术系伦理委员会的批准（申请号1873）。

设备和设置。 鉴于缺乏现有的开源耳内PPG平台，我们设计了一个定制的头戴式原型（见图1c），以收集耳内PPG信号与建立和负担得起的硬件组件。该原型由一个ESP 32微控制器组成，从左耳和右耳收集传感器数据。为了便于从耳内采集PPG信号（图2），我们制作了一个柔性PCB板，由MAXM 86161 (<https://www.maximintegrated.com/en/products/sensors/MAXM86161.html>) PPG传感器和ST-LSM6DSRX (<https://www.st.com/en/mems-and-sensors/lsm6dsrx.html>) IMU组成，如图1a所示。柔性PCB板通过I2C协议与ESP 32微控制器连接，用于数据采集。MAXM 86161是一款知名的3通道PPG传感器（绿色-520至550 nm，红色-660 nm，红外-880 nm），适合耳内传感应用。IMU连续记录3轴加速度计和3轴陀螺仪数据，以提供在进行面部表情或头部运动时发生的耳内运动的运动信号。两个传感器都以100 Hz的频率进行采样。如图1b所示，包含PPG传感器和IMU的柔性PCB涂覆有软硅胶，以类似于典型的耳塞，在佩戴设备时提供舒适性，并且在各种面部/头部运动期间在耳朵内保持牢固。我们使用透明的软硅胶来防止所采集的PPG信号中的任何失真。图2报告了该装置放置在耳道内的示意图。

PPG信号质量不仅受运动的影响，还受传感器配置的影响。通常，传感器允许改变影响所获取的信号并因此影响由传感器消耗的功率的若干参数。考虑到这种权衡，通常，信号质量的最佳参数在术语上不是最有效的

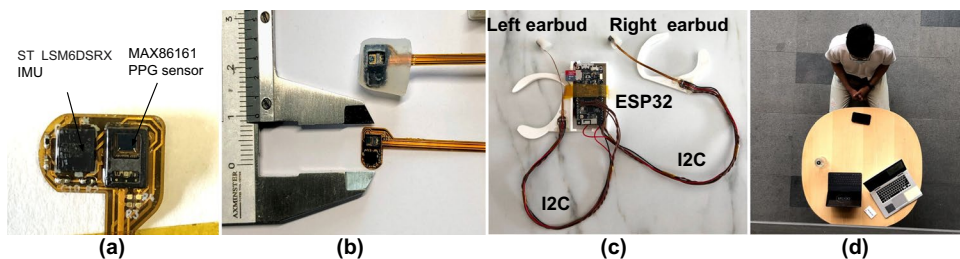


Fig. 1 (a) Flexible PCB implementation of our earbud featuring MAX86161 PPG sensor and a co-located ST LSM6DSRX IMU. (b) An in-ear soft earbud was realized by embedding the in-ear flexible PCB board into a transparent silicone mold. (c) Head-worn data acquisition device consisting of an ESP32 microcontroller collecting data from in-ear PPG and IMU sensors in the left and right ear. (d) A participant wearing our earbud-based prototype and taking part in the data collection protocol.

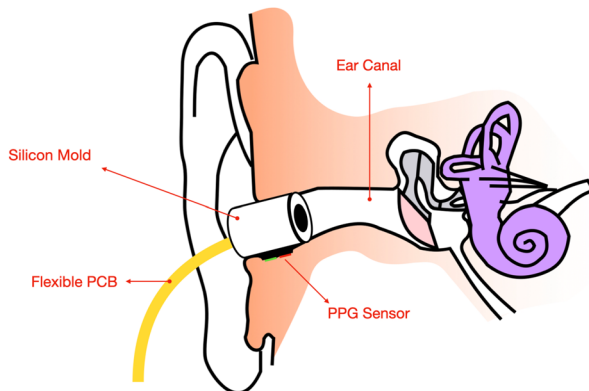


Fig. 2 Representation of the custom-built PPG ear tip inside the ear canal.

Conf.	LED Current (mA)	Pulse Width (us)	Integration Time (us)	Current Draw (mA)
1	16	21.3	14.8	1.62
2	32	21.3	14.8	1.81
3	16	123.8	117.3	2.66
4	32	123.8	117.3	3.78

Table 2. PPG parameters and relative sensor current draw.

of power consumption. To explore this aspect of PPG sensing, we configured our device to change the sensor parameters every 30 seconds. This way, by collecting data for 2 minutes for each motion session we could cycle through 4 different sets of configurations (Table 2). In particular, the MAXM86161 allows changing of three parameters: *LED current* which determines the brightness of the three LEDs, *pulse width* which is the time each LED is kept on during measurement, and *the integration time* which is the period during which the photodiode is active and sampling the reflected light. Notice that pulse width and integration time cannot be controlled individually and only 4 combinations of the two parameters are available in the sensor. As shown in Table 2, we have chosen 4 configurations that offer distinct power consumption profiles and should result in diverse SNR characteristics.

On the other hand, as a ground truth to collect vital signs from a reliable source, not affected by motion artifacts, we rely on a Zephyr Bioharness 3.0 (<https://www.zephyranywhere.com/>), a portable, medical-grade (FDA approved³⁰), ECG chest band. The participants wore the portable ground truth ECG band on their chests for the whole experiment.

Data collection protocol. After being briefed about the study, the participants wore our in-ear data collection device on the head placing the ear-tips in the left and right ear canal (Fig. 1) and the Zephyr Bioharness 3.0 ECG chest band. As in several prior works^{30,31}, the Zephyr acts as ground truth device in our data collection. Starting from a resting pose (participants sitting still without any motion), we progressively asked the participants to repetitively carry out individual movements. Notably, for the entire duration of each data collection session, one of the investigators stayed in the room with the participant (carefully observing social distancing and

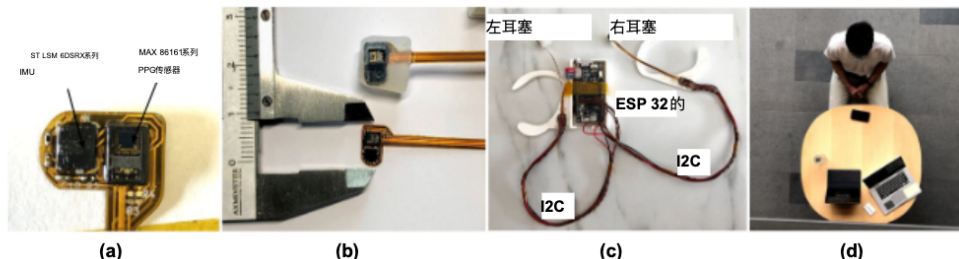


图1 (a) 采用MAX86161 PPG传感器和ST LSM 6DSRX IMU的耳塞的柔性PCB实现。(b)通过将入耳式柔性PCB板嵌入透明硅胶模具中，实现了入耳式软耳塞。(c)头戴式数据采集设备，由ESP32微控制器组成，从左耳和右耳的耳内PPG和IMU传感器收集数据。(d)一名参与者戴着我们的基于耳塞的原型，并参加了数据收集协议。

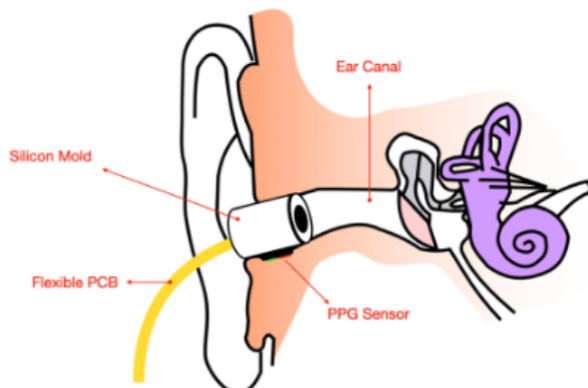


图2耳道内定制PPG耳塞的图示。

Conf	LED 电流 (mA)	Pulse Width (ms)	积分时间 (us)	电流消耗 (mA)
1	16	21.3	14.8	1.62
2	32	21.3	14.8	1.81
3	16	123.8	117.3	2.66
4	32	123.8	117.3	3.78

表2. PPG参数和相对传感器电流消耗。

电力消耗。为了探索PPG感测的这一方面，我们将我们的设备配置为每30秒改变传感器参数。这样，通过为每个运动会话收集2分钟的数据，我们可以循环通过4组不同的配置（表2）。特别是，MAXM86161允许改变三个参数：LED电流，它决定了三个LED的亮度，脉冲宽度，这是每个LED在测量过程中保持打开的时间，以及积分时间，这是光电二极管激活和采样反射光的时间。请注意，脉冲宽度和积分时间不能单独控制，传感器中只有4种两个参数的组合可用。如表2所示，我们选择了4种配置，它们提供不同的功耗曲线，并应产生不同的SNR特性。另一方面，作为从可靠来源收集生命体征的基础事实，不受运动伪影的影响，我们依靠Zephyr Bioharness 3.0 (<https://www.zephyrynywhere.com/>)，这是一种便携式医用级（FDA批准）ECG胸带。参与者在整个实验中将便携式地面真实ECG带佩戴在胸前。

数据收集方案。在简要介绍了这项研究后，参与者将我们的耳内数据收集设备戴在头上，将耳尖放在左右耳道中（图1）和Zephyr Bioharness 3.0 ECG胸带。与之前的几项工作一样，Zephyr 在我们的数据收集中充当地面实况设备。从休息姿势开始（参与者坐着不动），我们逐渐要求参与者重复进行个人运动。值得注意的是，在每次数据收集会话的整个持续时间内，其中一名研究人员与参与者呆在房间里（仔细观察社交距离和

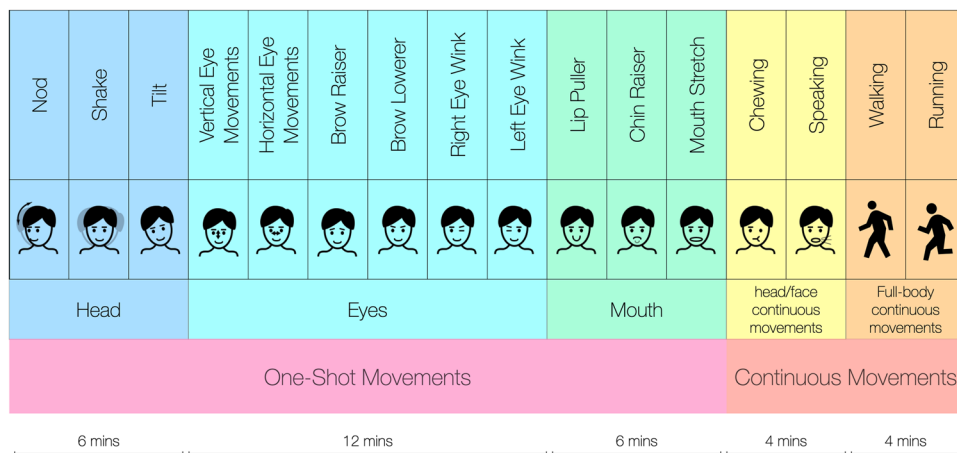


Fig. 3 Summary of the data collection protocol following a 2 minutes long still baseline. Each activity was performed for 2 minutes.

other COVID-19 precautions). We consider two main classes of motions: head/face movements and full-body movements. A summary of the data collection protocol (following the 2-minutes-long still baseline) is reported in Fig. 3. By looking at the inherent nature of the motions, head/face movements can be further categorized into *one-shot* and *continuous* movements.

- 1. One-shot motions:** One-shot motions are not normally performed continuously, and they are often performed in normal social interactions as well as in the form of psychosomatic tics. The selection process for the one-shot motion artifacts was informed by both anatomy principles²⁸ and previous work^{32–34}. In building our dataset, we look at Action Units (AUs) that entail the movement of the head, the eyes (and the adjacent muscles), and the mouth. Specifically, we selected: (1) *nod*; (2) *shake*; and (3) *tilt* as **head** movements. The **eye** movements chosen were: (4) *vertical eye movements*; (5) *horizontal eye movements*; (6) *brow raiser*; (7) *brow lowerer*; (8) *right eye wink*; and (9) *left eye wink*. Finally, we investigated: (10) *lip puller*; (11) *chin raiser*; and (12) *mouth stretch* as **mouth** movements. We instructed the participants to repeat the one-shot movements roughly every 5 seconds.
- 2. Continuous motions:** Besides, we also accounted for **head/face continuous movements** caused by common activities such as (13) *chewing*; and (14) *speaking*. Together with the one-shot movements, Continuous movements are quite unique to ear-worn devices. In fact, when performing these, the complex mesh of facial muscles moves substantially and, therefore, these activities are likely to cause significant deformations of the tissues in and around the ear.

Apart from head/face motions, we also considered **full-body activities** such as (15) *walking* and (16) *running*, which give rise to well-known sources of noise³⁵ in the PPG signal. The list of all the considered motion artifacts is reported in Table 4 and pictured in Fig. 4. Notably, before performing each and every motion, the investigator demoed each and every gesture/activity to the participants. Ultimately, for all the conditions but the full-body movements (walking and running), we followed the wearable device validation guideline stipulated by the Consumer Technology Association³⁶ and acquired PPG signals while seated in the upright position. During the *resting* condition, we instructed the participants to breathe normally without moving. The *speaking* condition consisted of a conversation with the investigator, where the participant described a recent event to the investigator. The *chewing* condition was assessed by recording PPG data while the participant was chewing gum. For the full-body motion conditions, the participants were asked to walk and run at a set pace on a treadmill. We set the treadmill's speed at 5kph and 8kph while walking and running, respectively. For each motion condition, we recorded 2 minutes of data, automatically changing the configuration of the PPG parameters every 30 seconds using the values described earlier. The length of the sessions was carefully chosen to be long enough to yield good-quality vital signs and yet not too tedious/harmful to the participants.

Collected data. We collected three types of data: (a) In-ear PPG signals from both left and right ear, (2) In-ear IMU signals from both left and right ear, and (3) Ground-truth heart rate data from Zephyr Bioharness 3.0 ECG chest band. Table 3 reports an overview of the characteristics of devices used to collect *EarSet* dataset. The table presents the type of data that was collected for each device as well as the sampling rate at which the data was collected. The table shows that *EarSet* contains data from 2 different devices (including an ECG ground truth as ground-truth information) placed on 2 unique body locations(in-ear and chest). The data from the accelerometer was available in both the body locations (ear and chest). Here now follows more details on the collected raw data.

- 1. In-ear PPG signals:** The in-ear PPG signals (19-bit analog to digital converted PPG values from MAXM86161) were collected using our custom head worn prototype at a sampling frequency of 100 Hz. The timestamps (in milliseconds resolution) are available for each PPG signal sample from both the left

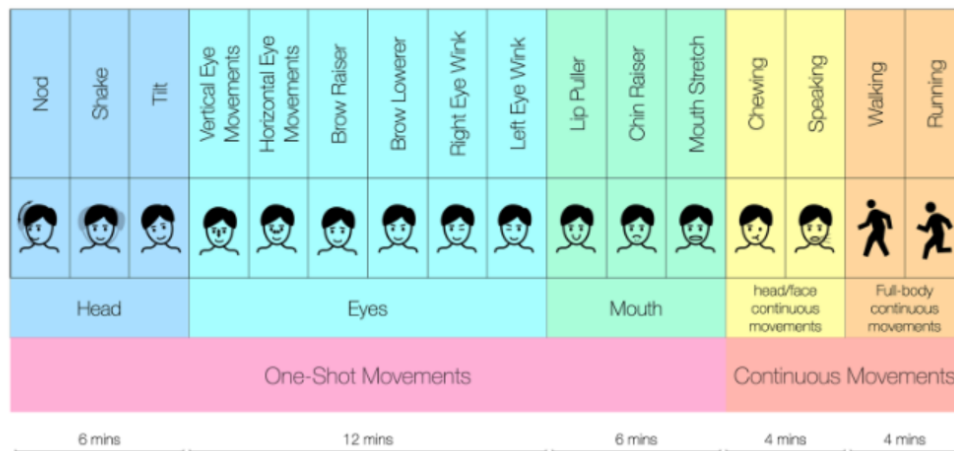


图3在2分钟长的静止基线之后的数据收集方案的总结。每个活动进行2分钟。

其他COVID-19预防措施）。我们考虑两个主要类别的运动：头/脸运动和全身运动。数据收集方案总结（2分钟静止基线后）见图3。通过观察运动的固有性质，头部/面部运动可以进一步分类为单次运动和连续运动。

1. 一次性动作：一次性动作通常不会连续进行，它们通常在正常的社会交往中以及以心身性抽搐的形式进行。一次性运动伪影的选择过程由解剖学原理和先前的工作告知。在构建数据集的过程中，我们研究了动作单元（AU），这些动作单元需要头部、眼睛（以及相邻的肌肉）和嘴巴的运动。具体来说，我们选择：(1) 点头；(2) 摆动；和(3) 倾斜作为头部运动。选择的眼球运动是：(4) 垂直眼球运动；(5) 水平眼球运动；(6) 眉毛抬高；(7) 眉毛降低；(8) 右眼眨眼；和(9) 左眼眨眼。最后，我们研究了：(10) 嘴唇拉；(11) 下巴抬起；和(12) 嘴部拉伸作为嘴部运动。我们指导参与者大约每5秒重复一次oneshot动作。
2. 连续运动：此外，我们还考虑了由com-fuse引起的头/脸连续运动。如(13) 咀嚼；(14) 说话。与一次性运动一起，连续运动对于耳戴式设备来说是非常独特的。事实上，当进行这些活动时，面部肌肉的复杂网格会大幅移动，因此，这些活动可能会导致耳朵内和周围组织的显著变形。

除了头部/面部运动之外，我们还考虑了全身活动，诸如(15) 步行和(16) 跑步，这给予PPG信号中的众所周知的噪声源。所有考虑的运动伪影列表如表4所示，如图4所示。值得注意的是，在执行每个动作之前，研究人员向参与者演示了每个手势/活动。最终，对于除了全身运动（步行和跑步）之外的所有条件，我们都遵循了消费者技术协会规定的可穿戴设备验证指南，并在直立坐姿时获取PPG信号。在休息状态下，我们指导参与者正常呼吸，不要移动。说话条件包括与研究者的对话，参与者向研究者描述最近发生的事件。通过记录参与者咀嚼口香糖时的PPG数据来评估咀嚼状况。对于全身运动条件，参与者被要求在跑步机上以固定的速度行走和跑步。我们将跑步机的速度分别设置为5公里/小时和8公里/小时。对于每个运动条件，我们记录了2分钟的数据，使用前面描述的值每30秒自动更改PPG参数的配置。会议的长度经过精心选择，以足够长的时间产生高质量的生命体征，但不会对参与者过于乏味/有害。

收集的数据。我们收集了三种类型的数据：(a) 来自左耳和右耳的耳内PPG信号，(2) 来自左耳和右耳的耳内IMU信号，以及(3) 来自Zephyr Bioharness 3.0 ECG胸带的地面上实心率数据。表3报告了用于收集EarSet数据集的设备特征的概述。该表列出了每种器械采集的数据类型以及采集数据的采样率。该表显示，EarSet包含来自放置在2个独特身体位置（耳内和胸部）的2个不同设备（包括ECG地面实况信息）的数据。来自加速度计的数据在两个身体位置（耳朵和胸部）都可用。以下是有关收集的原始数据的更多详细信息。

1. 耳内PPG信号：耳内PPG信号（来自MAXM86161的19位模数转换PPG值）使用我们的定制头戴式原型以100Hz的采样频率收集。时间戳（毫秒分辨率）可用于左侧和右侧的每个PPG信号样本

Sensor	Units/Range	Sampling Rate
Earable prototype (one per ear)		
Accelerometer	g {-2:+2}	100 Hz
Gyroscope	°/s {-500:+500}	100 Hz
PPG - green, infrared, and red channels	—	100 Hz
Zephyr Bioharness 3.0 chest band		
Heart Rate	beats per minute {25:240}	1 Hz
Breathing Rate	breaths per minute {3:70}	1 Hz
Core Temperature	degrees {10:60}	1 Hz
Posture	degrees from vertical {-180:180}	1 Hz
Activity vector magnitude units	g {-16:16}	1 Hz
Breathing Rate Amplitude	mV {0.25:15}	1 Hz
Heart Rate Variability	ms {0:65534}	1 Hz
ECG Amplitude	mV {0.25:15}	1 Hz

Table 3. Sensor data collected from each wearable device.

Class	Muscle Group	One-Shot	Action Units	Artifact Name
Still	n/a	n/a	Still	n/a
Head/Face	Head	✓	AU 53, 54	Nod
		✓	AU 51, 52	Shake
		✓	AU 55, 56	Tilt
	Eyes	✓	AU 63, 64	Vertical Eyes Movements
		✓	AU 61, 62	Horizontal Eyes Movements
		✓	AU 1, 2	Brow Raiser
		✓	AU 4	Brow Lowerer
		✓	AU 46	Right Eye Wink
		✓	AU 46	Left Eye Wink
	Mouth	✓	AU 12	Lip Puller
		✓	AU 17	Chin Raiser
		✓	AU 27	Mouth Stretch
		✗	AU 81	Chewing
		✗	AU 50	Speaking
Full-Body	n/a	✗	n/a	Walking
		✗	n/a	Running

Table 4. List of the considered motion artifacts and corresponding action unit (AU).

and the right ear. For each motion artifact, the PPG signals were collected for 2 minutes. Every 30 seconds, the PPG configuration was changed in the order reported in Table 2. As explained earlier, PPG signals were collected at three different wavelengths—green (530 nm), red (660 nm), and infrared (880 nm).

- In-ear IMU signals:** The in-ear IMU signals (both 3-axis accelerometer and gyroscope) were collected simultaneously with PPG signals using our custom head worn prototype at a sampling frequency of 100 Hz. The timestamps (with a milliseconds resolution) are available for each IMU record from both the left and the right ear. The IMU signals were also recorded continuously for each motion artifact session.
- Zephyr ground-truth data:** The Zephyr Bioharness 3.0 was worn by the participants on the chest and used to collect the ground-truth data. Specifically, the Zephyr provides heart rate (bpm), heart rate variability (ms) and ECG R-R interval (ms) at a sampling frequency of 1 Hz. In addition, the Zephyr provides raw 3-axis accelerometer data collected at a sampling frequency of 100 Hz. We also collect posture information (in degrees) at a sampling frequency of 1 Hz. The chest band also has a breathing sensor from which raw breathing waveform (25 Hz) and breathing/respiration rate (1 Hz) were collected.

PPG Features. Before delving into the detailed description of the dataset we collected, we summarize the signal processing techniques used with PPG signals. This lays the required signal processing foundation for understanding our dataset validation.

The most common biomarkers that can be derived from PPG are:

- Heart rate:** Peaks are detected from the AC component of the PPG signal to obtain the number of beats per minute. Typically the raw PPG signal is band-pass filtered between [0.4 Hz, 4 Hz] to obtain the AC component corresponding to the heart rate.

传感器	单位/范围	采样率
可佩戴原型（每只耳朵一个）		
加速计	g {-2: +2}	100 Hz
陀螺仪	° / s {-500: +500}	100 Hz
PPG - 绿色、红外和红色通道	-	100 Hz
Zephyr Bioharse 3.0胸带		
心率	每分钟心跳数	1 Hz
呼吸速率	每分钟呼吸次数{3: 70}	1 Hz
核心温度	度 (degree)	1 Hz
姿势	从垂直角度 (180度)	1 Hz
活动向量量值单位	(2016 - 06 - 16 00: 00: 00)	1 Hz
呼吸频率振幅	mV {0.25: 15}	1 Hz
心率变异性	ms {0: 65534}	1 Hz
ECG 幅度	mV {0.25: 15}	1 Hz

表3.从每个可穿戴设备收集的传感器数据。

类	肌群	单触发	产品名称	动作单元
仍	n/ a	n/ a	仍	n/ a
头部/脸部	Head	✓	Nod	AU 53, 54
		✓	摇	AU 51, 52
		✓	Tilt	AU 55, 56
	Eyes	✓	垂直眼动	AU 63, 64
		✓	水平眼动	AU 61, 62
		✓	眉毛提升器	Au 1, 2
		✓	下眉器	AU 4
		✓	右眼眨眼	AU 46
		✓	左眼眨眼	AU 46
	嘴	✓	拉唇器	AU 12
		✓	钦·雷泽	AU 17
		✓	嘴伸展	AU 27
		✗	口香	AU 81
		✗	发言	AU 50
全身	n/ a	✗	步行	n/ a
		✗	运行	n/ a

表4.所考虑的运动伪影和相应的动作单元 (Au) 的列表。

右耳。对于每个运动伪影，收集PPG信号2分钟。每隔30秒，PPG配置按照表2中报告的顺序进行更改。如前所述，PPG信号是在三个不同的波长-绿色 (530 nm)，红色 (660 nm) 和红外 (880 nm) 收集的。

- 入耳式IMU信号：使用我们的定制头戴式原型以100 Hz的采样频率同时收集耳内IMU信号（3轴加速度计和陀螺仪）和PPG信号。时间戳（具有毫秒分辨率）可用于来自左耳和右耳的每个IMU记录。还连续记录每个运动伪影会话的IMU信号。
- Zephyr地面实况数据：参与者将Zephyr Bioharse 3.0佩戴在胸前，用于收集地面实况数据。具体而言，Zephyr以1 Hz的采样频率提供心率 (bpm)、心率变异性 (ms) 和ECG R-R间期 (ms)。此外，Zephyr提供以100 Hz采样频率采集的原始3轴加速度计数据。我们还以1 Hz的采样频率收集姿势信息（以度为单位）。胸带还具有呼吸传感器，从该呼吸传感器收集原始呼吸波形 (25 Hz) 和呼吸/呼吸速率 (1 Hz)。

PPG 特征。在深入研究我们收集的数据集的详细描述之前，我们总结了PPG信号使用的信号处理技术。这为理解我们的数据集验证奠定了所需的信号处理基础。

可以从PPG中获得的最常见的生物标志物是：

- 心率：从PPG信号的AC分量检测峰值，以获得每分钟的心跳次数。典型地，原始PPG信号在[0.4Hz, 4Hz]之间被带通滤波以获得对应于心率的AC分量。

Head Movements	Eye Movements	Mouth Movements
	 Vertical Eye Movements	
Nod (Heads up and down)		Lip puller
	 Horizontal Eye Movements	
Tilt (Left or Right)	 Left and Right Eye Wink	Chin Raiser
	 Brow Raiser	 Mouth Stretch
Shake (Head left and right)	Brow Lowerer	

Fig. 4 Summary of the Facial Action Units (subset of the FACS) considered in the dataset⁶⁵. The individuals depicted provided consent for the open publication of the images.

2. **Oxygen saturation (SpO_2):** Oxygenated hemoglobin absorbs less red light whereas deoxygenated hemoglobin absorbs less infrared light. Thus, the ratio between red and infrared light intensities measured by the PPG sensor can be used to estimate SpO_2 (R) as follows:

$$R = \frac{R_{\text{red}}}{R_{\text{infrared}}} = \frac{AC_{\text{red}}/DC_{\text{red}}}{AC_{\text{infrared}}/DC_{\text{infrared}}} \quad (1)$$

3. **Heart rate variability (HRV):** Heart rate variability is measured as the time difference between adjacent peaks in a PPG signal.
4. **Respiration rate (RR):** A Synchrosqueezing transform (SST)³⁷ is applied on the raw PPG signals to extract the respiration component (0.1–0.9 Hz). The number of peaks in the resulting respiration component of the PPG signals corresponds to the respiration rate (breaths per minute). Besides, there are other techniques³⁸ using time domain and frequency domain features extracted from the PPG signal along with machine learning to estimate respiration rate.
5. **Blood pressure (BP):** Blood pressure is typically computed by placing PPG sensors at two locations on the same artery (say, finger and wrist) and then measuring the time taken by the pulse wave to travel from one PPG location to the other (pulse transit time). BP is inversely proportional to the pulse transit time obtained by calculating the peak time shifts between the two PPG sensors. In recent years, many machine learning and deep learning techniques^{39,40} have also been proposed to estimate blood pressure from the extracted PPG signal features.

As seen from the above biomarkers, the time domain signal features from the PPG signal are essential to estimate heart rate, heart rate variability as well as blood pressure. Some of the frequency domain features help in differentiating a normal sinus rhythm from an arterial fibrillation (AF) signal or an abnormal heart signal. In addition to the above-mentioned features, many techniques use features extracted from the first-order derivatives and the second-order derivatives of the PPG signal to compute arterial stiffness⁴¹ and blood pressure⁴⁰. The second-order derivative of a PPG signal provides useful information such as the location of the dicrotic notch, i.e., the time at which the diastolic peak occurs which provides information regarding the blood flow dynamics (systolic and diastolic phases).

Table 5 shows the main feature categories required for several critical health sensing applications. In addition to the PPG signal features mentioned earlier, useful physiological features marked in Fig. 5 can also be derived from the PPG signal⁴². The following list describes in more detail these main features which are also the ones we use in our technical validation of how various head and facial expressions affect in-ear PPG signals:

1. **Systolic phase:** The Amplitude of the systolic peak and the time at which the systolic peak is located in the PPG signal.

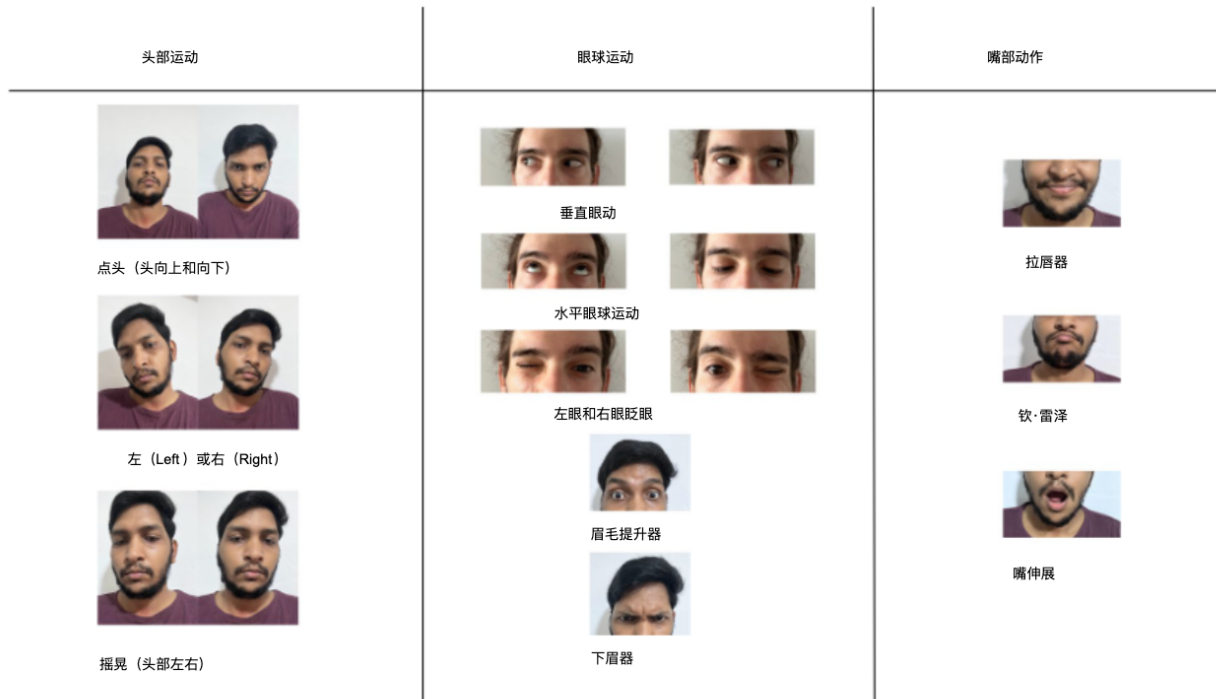


图4数据集中考虑的面部动作单位（FACS的子集）的总结。所描绘的个人同意公开发表这些图像。

2. 氧饱和度 (SpO)：氧合血红蛋白吸收较少的红光，而脱氧血红蛋白吸收较少的红外光。因此，由PPG传感器测量的红光和红外光强度之间的比率可以用于如下估计 SpO (R)：

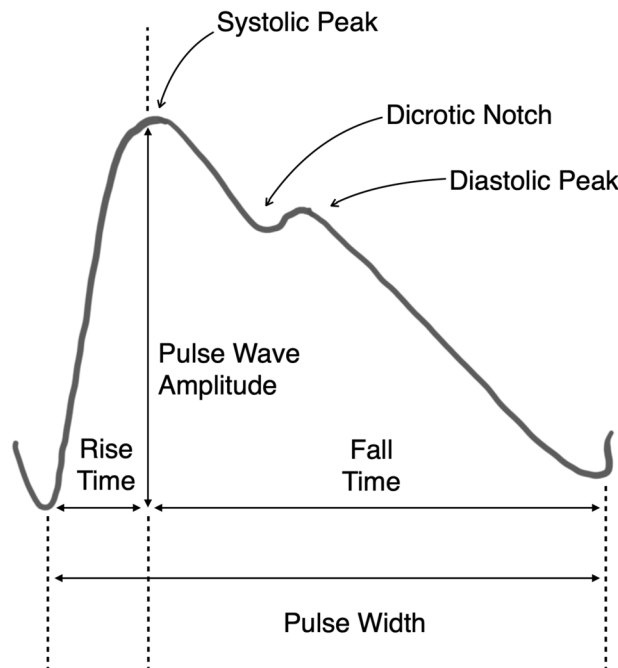
$$R = \frac{R_{\text{red}}}{R_{\text{红外}}} = \frac{AC_{\text{DC red}}}{AC_{\text{红外}} / DC_{\text{红外}}} \quad (1)$$

- 3. 心率变异性 (HRV)：心率变异性测量为PPG信号中相邻峰值之间的时间差。
- 4. 呼吸率 (RR)：对原始PPG信号应用同步压缩变换 (SST)，以提取呼吸分量 (0.1-0.9 Hz)。PPG信号的所得到的呼吸分量中的峰值的数量对应于呼吸速率（每分钟呼吸次数）。此外，还有其他技术使用从PPG信号中提取的时域和频域特征沿着机器学习来估计呼吸率。
- 5. 血压 (BP)：血压通常通过将PPG传感器放置在同一动脉上的两个位置（例如，手指和手腕）处并且然后测量脉搏波从一个PPG位置行进到另一个位置所花费的时间（脉搏传导时间）来计算。BP与通过计算两个PPG传感器之间的峰值时间偏移获得的脉搏传导时间成反比。近年来，还提出了许多机器学习和深度学习技术，以根据提取的PPG信号特征来估计血压。

从上述生物标志物可以看出，来自PPG信号的时域信号特征对于估计心率、心率变异性以及血压是必不可少的。一些频域特征有助于区分正常窦性心律与动脉纤维性颤动 (AF) 信号或异常心脏信号。除了上述特征之外，许多技术使用从PPG信号的一阶导数和二阶导数提取的特征来计算动脉硬度和血压。PPG信号的二阶导数提供有用的信息，例如重搏切迹的位置，即，舒张峰出现的时间，其提供关于血流动力学（收缩期和舒张期）的信息。表5显示了几个关键健康监测应用所需的主要功能类别。除了前面提到的PPG信号特征之外，还能够从PPG信号导出图5中标记的有用生理特征。以下列表更详细地描述了这些主要特征，这些特征也是我们在各种头部和面部表情如何影响耳内PPG信号的技术验证中使用的特征：

1. 收缩期：收缩峰的幅度和收缩峰位于PPG信号中的时间。

Applications	AC Component	DC Component	Time domain signal features	Frequency domain signal features	First order derivative features	Second order derivative features
Vital sign sensing (HR ⁵¹ , SpO ₂ ⁵² , BP ⁴⁰)	✓	✓	✓	✓	✓	✓
Heart rate variability (HRV) ^{53,54}	✓	✗	✓	✗	✗	✗
Respiration rate (RR) ^{55,56}	✓	✗	✗	✓	✗	✗
Sleep apnea ^{57,58}	✓	✗	✓	✗	✗	✗
Atrial Fibrillation ^{59,60}	✗	✗	✓	✓	✓	✓
Arterial Stiffness ^{41,61}	✗	✗	✓	✓	✓	✓
Energy expenditure ⁶²	✓	✗	✓	✓	✓	✓
Dehydration ^{63,64}	✗	✓	✗	✗	✗	✗

Table 5. Summary of PPG signal features essential for biomarkers as well as other health sensing applications.**Fig. 5** Typical time domain signal features extracted from a PPG signal.

2. **Diastolic phase:** The Amplitude of the diastolic peak and the time at which the diastolic peak is located in the PPG signal.
3. **Ratio between systolic and diastolic phase:** It is an indicator of the abnormalities in blood pressure. It is also referred to as the Augmentation index or Reflection index.
4. **Pulse width:** It is the time between the beginning and end of a PPG pulse wave. It correlates with our heart's systemic vascular resistance.
5. **Rise time:** The time between the foot of the PPG pulse and the systolic peak.
6. **Perfusion index (PI):** PI is the ratio of the pulsatile blood flow (AC component) to the non-pulsatile or static blood in peripheral tissue (DC component).
7. **Dominant frequency:** The dominant frequency of the PPG signal can be useful to give insights concerning the presence of artifacts at a different frequency outside the heart rate frequency band [0.4, 4 Hz].
8. **Spectral Kurtosis:** Also known as Frequency Domain Kurtosis, describes the distribution of the observed PPG signal frequencies around the mean and is a very useful indicator of the PPG signal quality.
9. **Peak-to-peak magnitude variance:** It is the variance of the difference between the pulse wave amplitude between two adjacent pulse waves.
10. **Peak-Time interval variance:** It is the variance of the pulse width between peaks of two adjacent PPG waves.

During the validation of our dataset, we show how the various motions and activities performed by the participants affect the features above. This demonstrates how head and facial motions could degrade the performance of health-related applications which rely on these features. We believe EarSet will help the research community in developing mitigation strategies for these motions and activities.

应用	AC 组件	DC 组件	时域 信号特征	频域 信号特征	一阶导数 特征	二阶 衍生工具特性
生命体征感知 (HR、SpO ₂ 、BP)	✓	✓	✓	✓	✓	✓
心率变异性 (HRV)	✓	✗	✗	✗	✗	✗
呼吸率 (RR)	✓	✗	✗	✗	✗	✗
睡眠呼吸暂停	✓	✗	✓	✗	✗	✗
房颤	✗	✗	✓	✓	✓	✓
动脉僵硬度	✗	✗	✓	✓	✓	✓
能量消耗	✓	✗	✓	✓	✓	✓
脱水	✗	✓	✓	✗	✗	✗

表5. PPG信号特征对于生物标志物以及其他健康感测应用至关重要的总结。

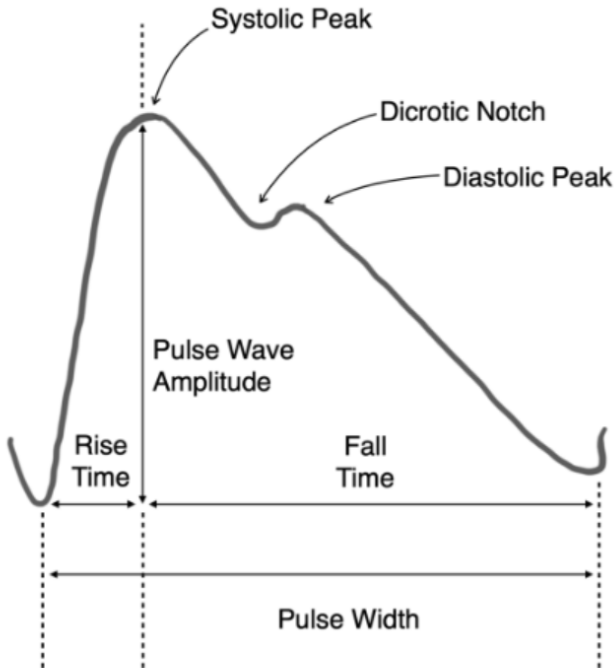


图5从PPG信号提取的典型时域信号特征。

2. 舒张期：舒张峰值的幅度和舒张峰值位于PPG信号中的时间。
3. 收缩期和舒张期之间的比值：它是血压异常的指标。它也被称为增强指数或反射指数。
4. 脉冲宽度：它是PPG脉冲波开始和结束之间的时间。它与我们心脏的全身血管阻力有关。
5. 上升时间：PPG脉搏的根部与收缩期峰值之间的时间。
6. 灌注指数 (PI)：PI是脉动血流 (AC分量) 与外周组织中的非脉动或静态血液 (DC分量) 的比率。
7. 主频率：PPG信号的主频率能够用于给予关于在心率频带[0.4, 4 Hz]之外的不同频率处的伪影的存在的洞察。
8. 光谱峰度：也称为频域峰度，描述了平均值周围观察到的PPG信号频率的分布，并且是PPG信号质量的非常有用的指标。
9. 峰-峰幅度方差：它是两个相邻脉搏波之间脉搏波幅度之差的方差。
10. 峰值-时间间隔方差：它是两个相邻PPG波的峰值之间的脉冲宽度的方差。

在验证数据集的过程中，我们展示了参与者执行的各种运动和活动如何影响上述特征。这表明头部和面部运动如何降低依赖于这些功能的健康相关应用程序的性能。我们相信EarSet将帮助研究界为这些运动和活动制定缓解策略。

Device	File	Column(s)	Description
EARBUDS	<ID>-<ACTIVITY>-imu-left.csv <ID>-<ACTIVITY>-imu-right.csv	timestamp	Timestamp in UNIX format with millisecond resolution.
		ax/gx	X-axis of accelerometer/gyroscope sensor.
		ay/gy	Y-axis of accelerometer/gyroscope sensor.
		az/gz	Z-axis of accelerometer/gyroscope sensor.
	<ID>-<ACTIVITY>-ppg-left.csv <ID>-<ACTIVITY>-ppg-right.csv	timestamp	Timestamp in UNIX format.
		green	PPG sensor green wavelength.
		ir	PPG sensor infrared wavelength.
		red	PPG sensor red wavelength.
ZEPHYR	<ID>_Summary.csv	Timestamp	Timestamp in UNIX format with millisecond resolution.
		HR	Heart rate measured from the ECG sensor.
		BR	Breathing rate is measured from a pressure sensor in the strap.
		CoreTemp	Core temperature.
		Posture	Posture: 0° = subject vertical, 90° = subject prone, -90° = subject supine, ±180° = subject inverted.
		Activity	Vector magnitude of the three axial acceleration magnitudes over the previous 1 second, sampled at 100 Hz.
		PeakAccel	Peak acceleration magnitude from the previous second.
		BRAmplitude	Breathing rate amplitude is used for internal development only.
		HRV	Heart rate variability.
		ECGAmplitude	Uncalibrated ECG amplitude measured from the peak of the R wave to the peak of the S wave of the QRS complex

Table 6. Description of the content of the folders named $P\#$ in the dataset. In this table, we explain only the most relevant files in the dataset. $<ID>$ represents the participant number from 0 to 29. $<ACTIVITY>$ is the artifact name as listed in Table 4.

Data Records

The raw data can be found at Zenodo⁴³. Data of each participant has been anonymized with the alphanumeric format: $P\#$. We refer to this as a participant identifier. The dataset contains a folder for each participant and an additional file, *Demographics.csv*, containing the demographics (e.g., gender, age) and skin tone of each participant in an anonymous format. Within each participant folder, there are two other folders, namely, *EARBUDS* and *ZEPHYR*, which contain the raw data obtained from each device during data collection. Table 6 provides an overview and description of the main files inside a participant folder.

Earbuds data. The IMU and PPG data are split into different files for each activity considered. The IMU sensor used the same configuration for the entire recording, while the PPG cycled through the four configurations described in Table 2. The transition before each configuration is marked by a line in the format #<timestamp>, current:<curr>, tint:<tint>, where <timestamp> is the UNIX time with milliseconds resolution, <curr> is the LED current in milli-Ampere and <tint> is the integration time in micro-seconds (this determines also the pulse width). All data points after this line have been collected with the new sensor configuration. Notice that the first configuration does not have such a line at the beginning.

To use the data collected from earbuds, one should first convert the raw ACC data to milli-g by multiplying it by 0.061 and the raw GYRO data to milli-dps (degrees per second) by multiplying with 17.5. This is to convert the raw data coming from the sensor from an integer format to a more usable format (i.e., milli-g and milli-dps). The PPG data does not require any conversion.

Zephyr data. The data from the Zephyr Bioharness is directly pre-processed by the device and provided at a 1 Hz granularity. Hence, data from this device can be used as is. Notably, in some instances, the first and last few data-points recorded by the Zephyr might present some artifacts due to the user wearing/removing the device.

Missing data. During the data collection, device malfunctions caused a minor loss of data. The PPG data relative to the mouth stretch activity for $P0$ and $P27$ is missing. Similarly, sensor configuration #4 is missing for $P9$ for the nod activity. In addition, the BRAmplitude data field recorded by the Zephyr is not present for users $P17$, $P26$, $P27$, $P28$, and $P29$. Finally, users $P3$, $P4$, $P7$, $P8$, and $P10$ have corrupted Zephyr data (notably, their IMU and PPG data from our prototype are still perfectly usable).

Technical Validation

In this section, we perform a preliminary analysis of the collected data to evaluate its technical validity. We independently processed the PPG signals from the 3 channels (green, red, infrared) recorded from the left and the right ears. The acquired PPG signals from the left and right ear were aligned in the time axis and stored in Pandas Data Frames. Each Data Frame is then re-sampled at 100 Hz to ensure a consistent sampling rate. The start and the end of each Data Frame were trimmed to ensure that each data frame has the same length. Note

装置	File	色谱柱	描述
耳塞	-imu-left.csv -imu-right.csv	时间截	UNIX格式的时间戳，具有毫秒分辨率。
		ax/gx	加速度计/陀螺仪传感器的X轴。
		gy/gy	加速度计/陀螺仪传感器的Y轴。
		az/az	加速度计/陀螺仪传感器的Z轴。
		时间截	UNIX格式的时间戳。
	-ppg-left.csv -ppg-right.csv	绿色	PPG传感器绿色波长。
		ir	PPG传感器红外波长。
		red	PPG传感器红色波长。
ZEPHYR	_摘要.csv	时间截	UNIX格式的时间戳，具有毫秒分辨率。
		HR	从ECG传感器测量心率。
		BR	呼吸率是从皮带中的压力传感器测量的。
		核心温度	核心温度。
		姿势	体位：0° =受试者垂直，90° =受试者俯卧，-90° =受试者仰卧，±180° =受试者倒置。
		活动	在100 Hz下采样的前1秒内三个轴向加速度幅值的矢量幅值。
		峰值加速度	前一秒的加速度峰值。
		BRAmplitude	呼吸频率振幅仅用于内部开发。
		HRV	心率变异性。
		ECG振幅	从QRS波群的R波峰到S波峰测量的未校准ECG振幅

表6.数据集中名为P# 的文件夹内容的描述。在此表中，我们仅解释数据集中最相关的文件。表示参与者编号，从0到29。是表4中列出的工作名称。

数据记录

原始数据可在Zenodo找到。每位参与者的数据均采用字母数字格式匿名化：P#。我们将其称为参与者标识符。数据集包含每个参与者的文件夹和包含人口统计数据（例如，性别、年龄）和肤色。在每个参与者文件夹中，还有另外两个文件夹，即EARBUDS和ZEPHYR，其中包含数据收集期间从每个器械获得的原始数据。表6提供了参与者文件夹中主要文件的概述和描述。

耳机数据。对于所考虑的每个活动，IMU和PPG数据被分成不同的文件。IMU传感器在整个记录过程中使用相同的配置，而PPG循环通过表2中描述的四种配置。每个配置之前的转换由格式为#，current：，tint：的线标记，其中是具有毫秒分辨率的UNIX时间，是以毫安为单位的LED电流，是以微秒为单位的积分时间（这也决定了脉冲宽度）。这条线之后的所有数据点都是用新的传感器配置收集的。请注意，第一个配置的开头没有这样的行。要使用从耳塞收集的数据，首先应将原始ACC数据乘以0.061转换为毫g，将原始GYRO数据乘以17.5转换为毫dps（每秒度）。这是为了将来自传感器的原始数据从整数格式转换为更可用的格式（即，毫-g和毫-dps）。

PPG数据不需要任何转换。

和风数据。来自Zephyr Bioharness 的数据直接由设备进行预处理，并以1 Hz的粒度提供。因此，来自该设备的数据可以按原样使用。值得注意的是，在某些情况下，Zephyr 记录的第一个和最后几个数据点可能会由于用户佩戴/移除设备而呈现一些伪影。

数据缺失。在数据收集过程中，器械故障导致轻微数据丢失。P0 和P27 时与口部伸展活动相关的PPG 数据缺失。类似地，节点活动的P9 缺少传感器配置#4。此外，对于用户P17、P26、P27、P28 和P29，不存在由Zephyr 记录的BRAmplitude 数据字段。最后，用户P3、P4、P7、P8 和P10的Zephyr 数据已经损坏（值得注意的是，他们的IMU和PPG 数据仍然可以完美使用）。

技术验证

在本节中，我们对收集的数据进行初步分析，以评估其技术有效性。我们独立地处理从左耳和右耳记录的来自3个通道（绿色、红色、红外）的PPG信号。从左耳和右耳采集的PPG信号在时间轴上对齐并存储在Pandas数据帧中。然后，每个数据帧以100 Hz重新采样，以确保一致的采样率。每个数据帧的开始和结束都经过修剪，以确保每个数据帧具有相同的长度。注意

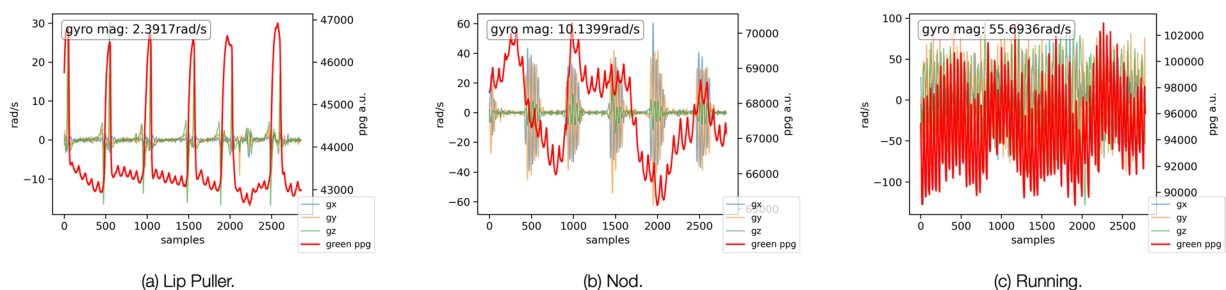


Fig. 6 Samples of green PPG and IMU (gyroscope) data under different motion artifacts.

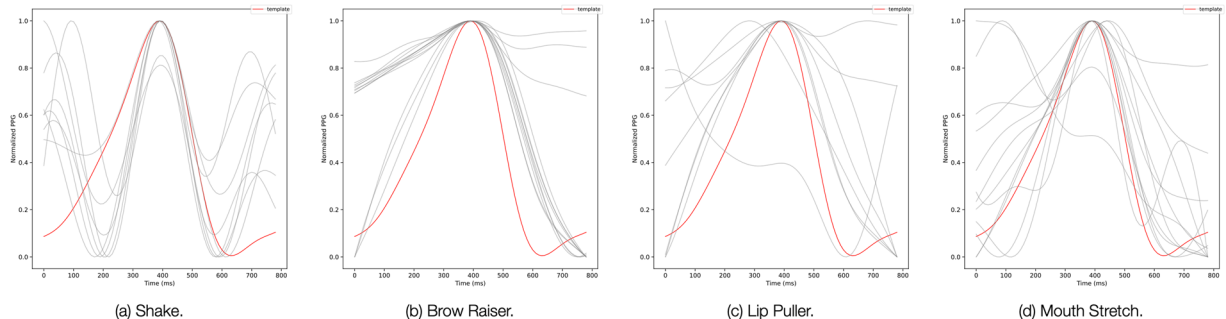


Fig. 7 Template matching of PPG pulses from user 12 for four different motions. The red line represents the template pulse computed with data from the still condition. The gray lines are the pulses from different motion conditions.

that our preliminary exploration only focuses on the 4th set of LED configuration parameters (LED current $32mA$; pulse width $123.8\mu s$; integration time $117.3\mu s$), as described in our Methods.

Dataset outlook and template matching. Firstly, we analysed EarSet to study how each facial motion artifacts appear unique in the collected in-ear PPG signals. In Fig. 6, we can appreciate at a glance how two diverse facial movements, such as lip puller (a) and nod (b), have a very different impact on the PPG trace when compared to a full-body movement like running (c)—in which the signal is dominated by the running cadence rather than by the cardiac signal. Notably, we can observe substantial differences even among the two facial movements: while the impact of the lip puller appears very localized and aligned with the motion (as we can see from the variations along the gyroscope axes), the nod seems to have a more prolonged impact on the DC component of PPG trace. By manually inspecting the data, we noticed that for a few [participant, motion] combinations, the PPG was not affected by artifacts. In particular, the vertical and horizontal movement of the eyes did not cause any artifact on the PPG signals. This is due to the limited involvement of the facial muscles, especially of those near the ears, during eye movements. Similarly, for the left and right eye wink motions, some participants could not perform the motion with both eyes or not at all. In other cases, the wink was subtle and hence did not result in any artifact in the corresponding PPG signal. For the rest of the analysis, we filtered out these [participant, motion] combinations for which the PPG was not affected by motion.

To deepen our investigation, and gain a better visual understanding of how the various motion artifacts affect the morphology of the PPG pulses, we relied on a template matching analysis⁴². In doing so, we crafted a template pulse by taking the average of all the pulses of each user when still. We then plot the template pulse in red and use it as a reference against all the PPG pulses present in each motion session (plotted in gray). Figure 7 depicts the template matching analysis for shake (a), brow raiser (b), lip puller (c), and mouth stretch (d). The plots show how each of the considered movements affects the morphology of the PPG pulse differently, resulting in subtle, yet notable artifacts. Many applications rely on morphological features computed on the PPG signals⁴². Hence, such artifacts in the morphology of each pulse could lead to erroneous vitals estimation. We believe that our dataset represents a good resource for a more in-depth study and characterization of this issue for an emerging class of devices—earables equipped with health-related sensors.

Handcrafted metrics extraction from EarSet. We sought to proceed with our exploration of the dataset by extracting handcrafted features commonly derived from PPG signals for various health sensing applications listed in our Methods. For all the PPG signal metrics excluding Perfusion Index, we apply a 4th-order Butterworth band-pass filter (low-cut = $0.4Hz$, high-cut = $4Hz$) for signal smoothening. To facilitate a fair comparison of the PPG signal metrics for each facial motion artifact available in EarSet, we normalized their values using a standard min-max normalization. We chose to independently normalize the metric values for each user's motion artifacts. Specifically, normalizing every user independently allows us to retain the subject-dependent motion artifact characteristics as well as the unique blood vessel morphology of each user.

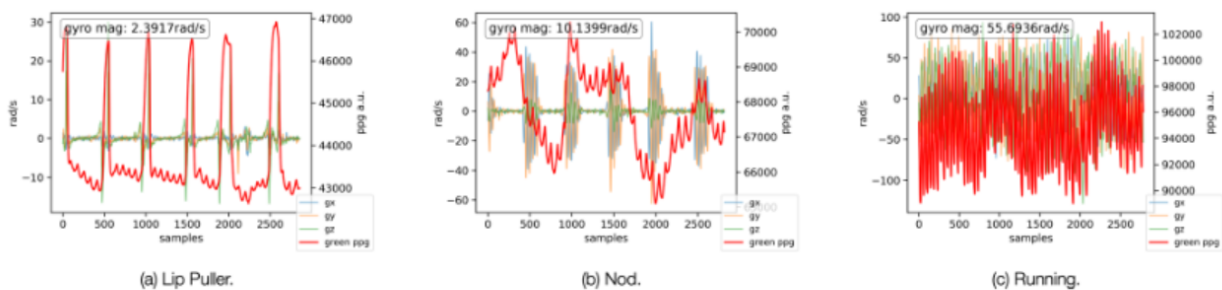


图6不同运动伪影下的6个绿色PPG和IMU（陀螺仪）数据样本。

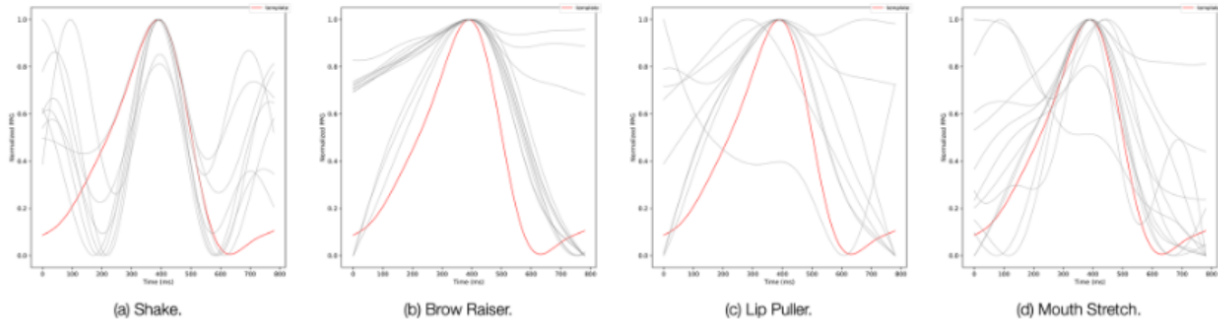


图7针对四个不同运动的来自用户12的PPG脉冲的模板匹配。红线表示用静止条件下的数据计算的模板脉冲。灰色线是来自不同运动条件的脉冲。

我们的初步探索只集中在第四组LED配置参数（LED电流32 mA;脉冲宽度123.8 μ s;积分时间117.3 μ s），如我们的方法中所述。

数据集前景和模板匹配。首先，我们分析EarSet来研究每个面部运动伪影如何在所收集的耳内PPG信号中出现独特的。在图6中，我们可以一眼看出两种不同的面部运动，例如拉唇（a）和点头（B），当与全身运动（例如跑步（c））相比时，对PPG迹线具有非常不同的影响，其中信号由跑步节奏而不是由心脏信号主导。值得注意的是，我们甚至可以在两个面部运动中观察到实质性差异：虽然嘴唇拉动器的影响看起来非常局部化并且与运动对齐（如我们可以从沿着陀螺仪轴的变化中看到的），但是点头似乎对PPG迹线的DC分量具有更长时间的影响。通过手动检查数据，我们注意到，对于一些[参与者，运动]组合，PPG不受伪影影响。特别是，眼睛的垂直和平运动不会对PPG信号造成任何伪影。这是由于在眼球运动过程中面部肌肉的参与有限，特别是那些靠近耳朵的肌肉。类似地，对于左眼和右眼眨眼运动，一些参与者不能用双眼执行运动或根本不能执行运动。在其他情况下，闪烁是微妙的，因此不会导致相应PPG信号中的任何伪影。对于分析的其余部分，我们过滤掉PPG不受运动影响的这些[参与者，运动]组合。

为了加深我们的研究，并获得更好的视觉理解的各种运动伪影如何影响形态的PPG脉冲，我们依赖于模板匹配分析。在此过程中，我们通过计算每个用户静止时所有脉冲的平均值来制作模板脉冲。然后，我们用红色绘制模板脉冲，并将其用作每个运动会话中存在的所有PPG脉冲的参考（用灰色绘制）。图7描绘了针对摇动（a）、眉毛提升（b）、嘴唇提拉（c）和嘴拉伸（d）的模板匹配分析。这些图显示了所考虑的每种运动如何不同地影响PPG脉冲的形态，从而导致细微但明显的伪影。许多应用依赖于在PPG信号上计算的形态特征。因此，每个脉冲的形态中的这种伪影可能导致错误的生命体征估计。我们相信，我们的数据集代表了一个很好的资源，为更深入的研究和表征这个问题的新兴类别的设备，配备了健康相关的传感器。

从EarSet手工提取指标。我们试图通过提取通常源自PPG信号的手工特征来继续我们对数据集的探索，用于我们的方法中列出的各种健康感测应用。对于除灌注指数外的所有PPG信号度量，我们应用4阶巴特沃思带通滤波器（低截=0.4 Hz，高截=4 Hz）进行信号平滑。为了便于对EarSet中可用的每个面部运动伪影的PPG信号度量进行公平比较，我们使用标准的最小值-最大值归一化对其值进行归一化。我们选择独立地归一化每个用户的运动伪影的度量值。具体而言，独立地归一化每个用户允许我们保留受试者相关的运动伪影特性以及每个用户的独特血管形态。

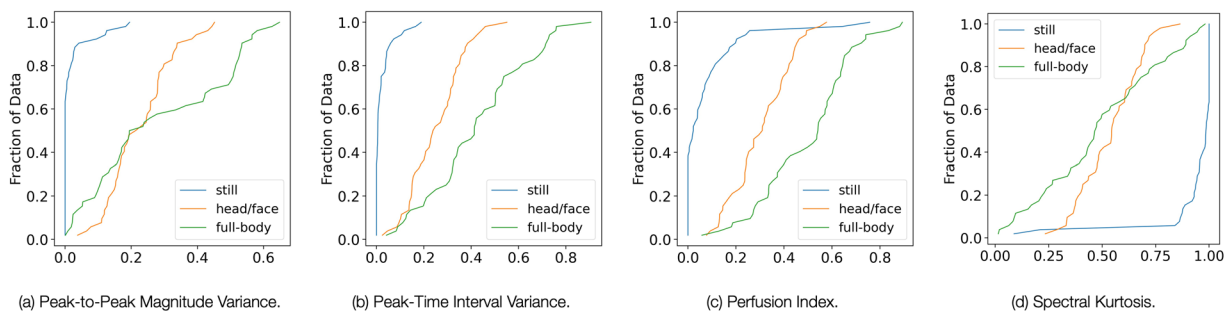


Fig. 8 Empirical Cumulative Distribution Function (ECDF) of how the various classes of motion artifacts impact some of the handcrafted metrics extracted from PPG.

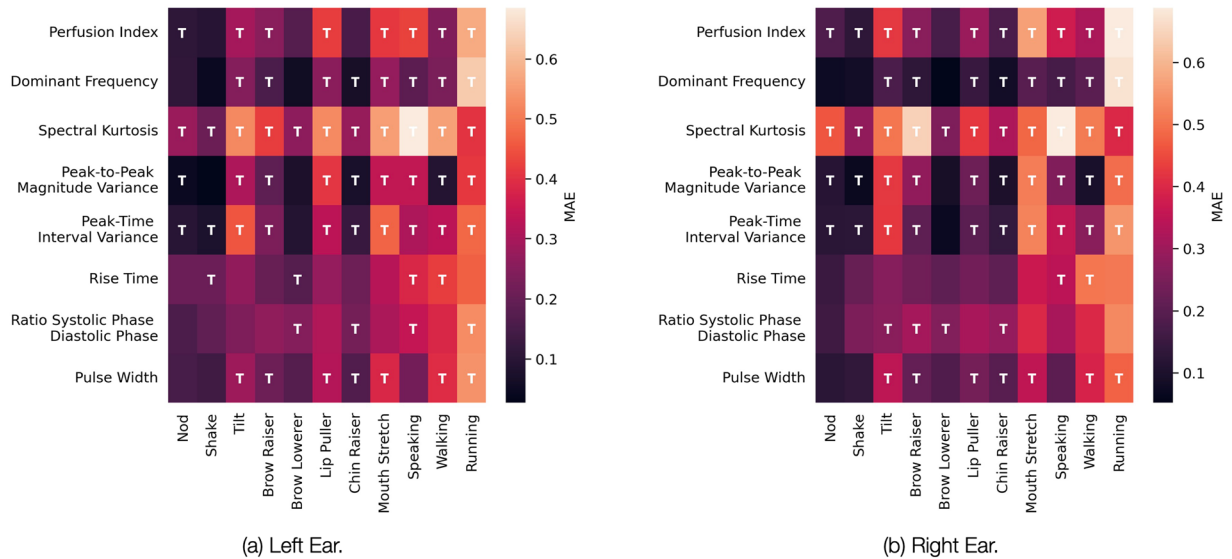


Fig. 9 Heatmaps of how the various motion artifacts impact the handcrafted metrics extracted from the green PPG signal ((a) left ear; (b) right ear). The values reported in the heatmaps are the Mean Absolute Error (MAE) with respect to the still baseline. The heatmaps' cells are annotated with a T whenever there is a statistically significant difference between the still baseline signal and the MA-corrupted one ($p < 0.05$).

Figure 8 reports the empirical cumulative distribution function (ECDF) of how head/face and full-body movements impact the Peak-to-Peak Magnitude Variance (a), Peak-Time Interval Variance (b), Perfusion Index (c), and the Spectral Kurtosis (d) of the in-ear PPG signal. Similar patterns can be observed for other metrics. For this analysis, we considered the normalized PPG signal metrics computed from both the left and the right ear for all the users. We can observe that the PPG signal metrics for the “still” situation remain consistent across the entire population. On the other hand, the facial(head/face) and full-body movements appear to have more widespread distributions as well as different patterns. This is especially true for full-body movements. Notably, the findings of the spectral kurtosis analysis (d) are also aligned to the literature⁴², showing higher values for clean PPG signal. This can be explained by the presence of sharper peaks in the Fourier spectrum of clean (still in our case) PPG. These preliminary results suggest that different motion categories (i.e., head/face and full-body) create diverse artifacts in the PPG signal, and therefore it might be necessary to adopt dedicated approaches when applying signal filtering techniques. Our preliminary analysis of EarSet show that our dataset is a good source to start exploring this avenue.

Finally, We studied whether it is possible to spot differences between the individual motions using the collected PPG signals in EarSet. We began by looking at the Mean Absolute Error (MAE) between all the PPG signal metrics extracted under the various motion artifact and the “still” stationary PPG signal baseline. As we can see from Fig. 9, for the majority of the PPG signal metrics, there are statistically significant differences between the still baseline and most of the artifacts. As expected, more intense head/face movements, like tilt and mouth stretch, yield greater differences in the signal metrics computed against the still baseline. This is much more evident while looking at full-body movements. Besides, a comparison of data from the left (??) and right (??) ear hints at differences between the PPG signals collected from the two ears. Multi-site PPG signals from the ears have been largely understudied so far. We believe our dataset is the perfect starting point to further explore this area.

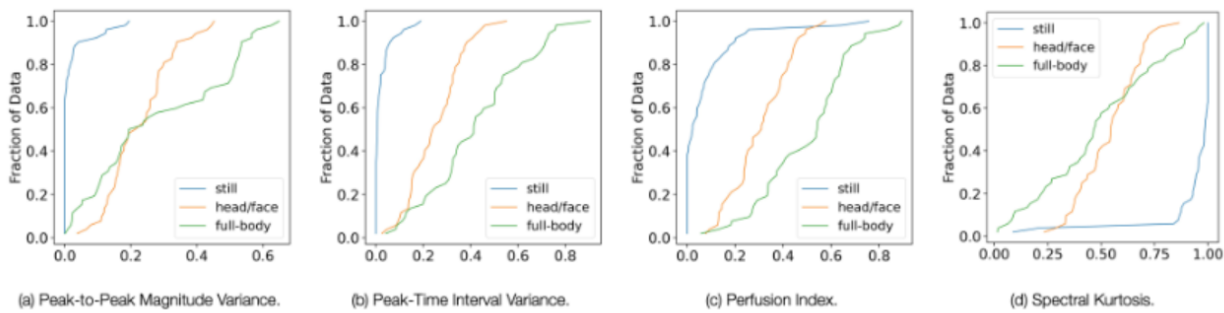


图8经验累积分布函数 (ECDF)，说明各种运动伪影如何影响从PPG中提取的一些手工度量。

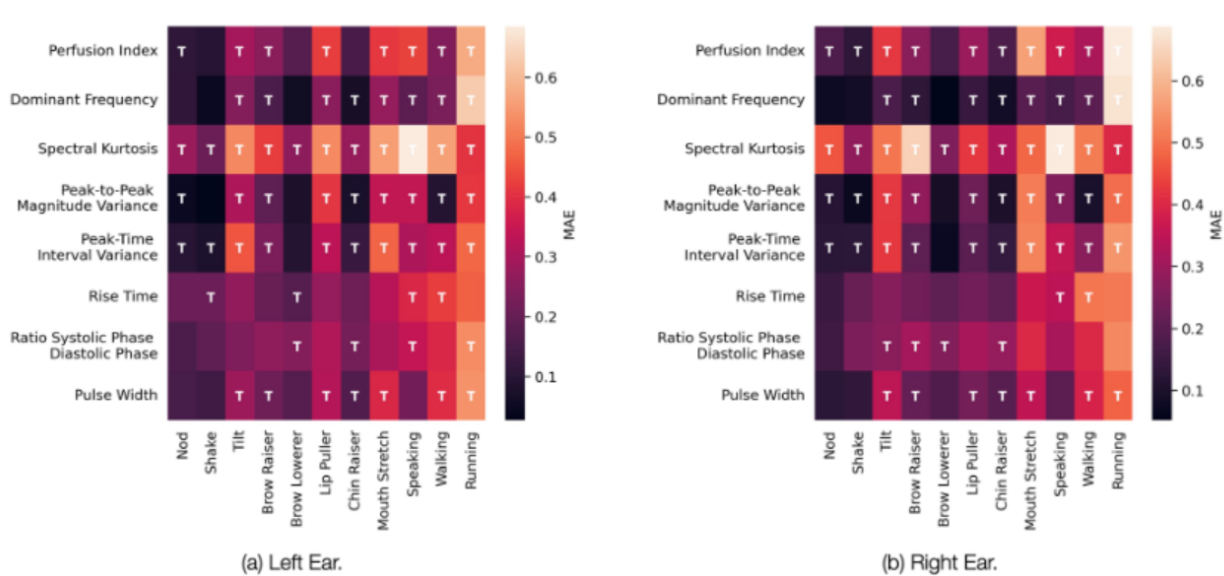


图9各种运动伪影如何影响从绿色PPG信号提取的手工度量的热图 ((a) 左耳; (B) 右耳)。热图中报告的值是相对于静止基线的平均绝对误差 (MAE)。只要在静止基线信号和MA破坏的信号之间存在统计学显著差异 ($p < 0.05$)，热图的单元格就用T注释。

图8报告了头部/面部和全身运动如何影响耳内PPG信号的峰-峰幅度方差 (a)、峰-时间间隔方差 (b)、灌注指数 (c) 和谱峰度 (d) 的经验累积分布函数 (ECDF)。对于其他指标，可以观察到类似的模式。对于该分析，我们考虑了从所有用户的左耳和右耳计算的归一化PPG信号度量。我们可以观察到，“静止”情况的PPG信号度量在整个群体中保持一致。另一方面，面部(头/脸)和全身运动似乎具有更广泛的分布以及不同的模式。这对于全身运动来说尤其如此。值得注意的是，频谱峰度分析 (d) 的结果也与文献一致，表明干净PPG信号的值更高。这可以通过在干净(仍然在我们的情况下)PPG的傅立叶光谱中存在更尖锐的峰来解释。这些初步结果表明，不同的运动类别(即，头部/面部和全身)在PPG信号中产生不同的伪影，并且因此在应用信号滤波技术时可能需要采用专用的方法。我们对EarSet的初步分析表明，我们的数据集是开始探索这一途径的良好来源。

最后，我们研究了是否有可能使用EarSet中收集的PPG信号来发现个体运动之间的差异。我们首先查看在各种运动伪影下提取的所有PPG信号度量与“静止”静止PPG信号基线之间的平均绝对误差 (MAE)。从图9中可以看出，对于大多数PPG信号度量，静态基线和大多数伪影之间存在统计学显著差异。正如预期的那样，更强烈的头部/面部运动，如倾斜和嘴巴伸展，在相对于静止基线计算的信号度量中产生更大的差异。这一点在观察全身运动时更为明显。此外，从左(?)右(?)耳朵暗示从两只耳朵收集的PPG信号之间的差异。到目前为止，来自耳朵的多部位PPG信号在很大程度上尚未得到充分研究。我们相信我们的数据集是进一步探索这一领域的完美起点。

Usage Notes

Data pre-processing. The data recorded from the Zephyr does not require additional processing as they are already pre-processed (with the exception of the ECGAmplitude and the BRAmplitude, which can be easily pre-processed using NeuroKit library).

However, the data collected from our earable prototype requires pre-processing. Firstly, the raw accelerometer data has to be converted to milli-g units by multiplying with 0.061, and the raw gyroscope data has to be converted to milli-dps (degrees per second) by multiplying with 17.5. This converts the raw IMU sensor data from an integer format to a more usable/standard format (i.e., milli-g and milli-dps). We then remove the direct current (DC) offset from the gyroscope data by applying a Butterworth band-pass filter (0.4–4 Hz cutoff). Secondly, the PPG signals can be pre-processed using bandpass filtering options available in HeartPy or NeuroKit libraries to extract HR, SpO₂, etc.

EarSet dataset. The EarSet dataset is available in⁴³. Convenient libraries to pre-process and clean the physiological signals include HeartPy (<https://python-heart-rate-analysis-toolkit.readthedocs.io/en/latest/>) to extract heart rate data from PPG or ECG sensors, NeuroKit (<https://neurokit2.readthedocs.io/en/latest/index.html>) and BrainFlow (<https://github.com/brainflow-dev/brainflow>) to analyze PPG and ECG signals.

We believe that the EarSet dataset will foster research of new solutions to problems such as:

- *Motion Artifacts Filtering:* The dataset enables the exploration of how subtle head and face motions affect in-ear IMU and PPG signals. Firstly, this allows studying what kind of facial movements cause significant degradation of the PPG signals and how they might affect the accuracy of vital signs estimation. Secondly, the dataset will motivate the design of sophisticated filtering techniques for in-ear PPG signals - targeted at eliminating head and facial motion artifacts.
- *Sensor Location:* EarSet offers a unique opportunity to study whether the availability of PPG sensors in both ears could improve the estimation of vital signs. Having access to independent streams of PPG signals from the left and right ears could highlight asymmetries in the way people perform head and facial movements. These findings could be exploited to design improved signal-filtering approaches.
- *Sensor Configuration:* Given the need for low power consumption in future earable devices, the dataset allows the exploration of how different PPG hardware configurations (including 3 wavelengths), each with specific power requirements, affect the acquired PPG signal quality. This has important implications for the design of future devices and processing pipelines.
- *State-of-the-art Comparison:* The dataset contains several physiological measurements from ECG signals measured using a Zephyr Bioharness 3.0 chest strap. This enables validation and benchmarking of vital signs estimation methods applied to in-ear data with state-of-the-art methods from commercial devices unaffected by head/facial motions.

While the EarSet dataset opens up novel opportunities for earable devices, our approach still has a few limitations and presents opportunities for further improvements. Our focus is to offer a dataset to investigate the impact of head/face motions, in addition to full-body activities, on in-ear PPG signal quality and vital signs estimation. Skin tone is an additional factor that could affect data quality³⁵. Although EarSet offers diversity in skin tones, the acquired data does not follow a uniform distribution among the six categories of pigmentation²⁹. Future work will consider expanding the dataset to include additional participants to uniformly cover all skin tones.

All our participants were healthy at the time of the data collection and had no heart-related conditions. Future data collection efforts will consider participants with underlying conditions that could affect the morphology of the PPG signal even without the presence of motion-related artifacts. Correctly distinguishing the two cases would significantly increase the trustworthiness of earable devices beyond commercial settings - with the potential to be applied in clinical settings. Additionally, manual assessment of the PPG signal quality from experts in the field would complement the dataset, enabling the development of automatic pipelines to estimate expert-grade clinical assessments.

Code availability

We provide the raw data files obtained during the data collection structured by a user identifier. We did not implement any specialized code to pre-process the data.

Received: 9 March 2023; Accepted: 17 November 2023;

Published online: 01 December 2023

References

1. Castaneda, D., Esparza, A., Ghamari, M., Soltanpur, C. & Nazeran, H. A review on wearable photoplethysmography sensors and their potential future applications in health care. *International journal of biosensors & bioelectronics* **4**, 195 (2018).
2. Imanaga, I., Hara, H., Koyanagi, S. & Tanaka, K. Correlation between wave components of the second derivative of plethysmogram and arterial distensibility. *Japanese heart journal* **39**, 775–784 (1998).
3. Suganthi, L., Manivannan, M., Kunwar, B. K., Joseph, G. & Danda, D. Morphological analysis of peripheral arterial signals in takayasu's arteritis. *Journal of clinical monitoring and computing* **29**, 87–95 (2015).
4. Allen, J. Photoplethysmography and its application in clinical physiological measurement. *Physiological measurement* **28**, R1 (2007).
5. Zhao, T. *et al.* Trueheart: Continuous authentication on wrist-worn wearables using ppg-based biometrics. In *IEEE INFOCOM 2020-IEEE Conference on Computer Communications*, 30–39 (IEEE, 2020).
6. Lee, B.-G., Jung, S.-J. & Chung, W.-Y. Real-time physiological and vision monitoring of vehicle driver for non-intrusive drowsiness detection. *IET communications* **5**, 2461–2469 (2011).

用法注释

数据预处理。从Zephyr记录的数据不需要额外处理，因为它们已经进行了预处理（ECG振幅和BRAmplitude除外，可以使用NeuroKit库轻松进行预处理）。

然而，从我们的earable原型收集的数据需要预处理。首先，原始加速度计数据必须通过乘以0.061转换为毫g单位，原始陀螺仪数据必须通过乘以17.5转换为毫dps（每秒度）。这将原始IMU传感器数据从整数格式转换为更可用/标准的格式（即，毫-g和毫-dps）。然后，我们通过应用巴特沃思带通滤波器（0.4-4 Hz截止）从陀螺仪数据中去除直流（DC）偏移。其次，可以使用HeartPy或NeuroKit库中可用的带通滤波选项来预处理PPG信号，以提取HR、SpO等。

EarSet数据集。 EarSet数据集在中提供。用于预处理和清理生理信号的便利库包括HeartPy (<https://python-heart-rate-analysis-toolkit.readthedocs.io/en/latest/>)，用于从PPG或ECG传感器提取心率数据，NeuroKit (<https://neurokit2.readthedocs.io/en/latest/index.html>) 和BrainFlow (<https://github.com/brainflow-dev/brainflow>) 用于分析PPG和ECG信号。

我们相信EarSet数据集将促进对问题的新解决方案的研究，例如：

- **运动伪影过滤：**该数据集可以探索头部和面部运动如何影响耳内IMU和PPG信号。首先，这允许研究什么样的面部运动导致PPG信号的显著退化以及它们如何可能影响生命体征估计的准确性。其次，该数据集将激励设计用于耳内PPG信号的复杂滤波技术-旨在消除头部和面部运动伪影。
- **传感器位置：**EarSet提供了一个独特的机会来研究双耳中PPG传感器的可用性是否可以改善生命体征的估计。从左耳和右耳获得独立的PPG信号流可以突出人们执行头部和面部运动的方式的不对称性。
- **这些发现可以用来设计改进的信号过滤方法。**
- **传感器配置：**考虑到未来可穿戴设备对低功耗的需求，该数据集允许探索不同的PPG硬件配置（包括3个波长）如何影响采集的PPG信号质量，每个配置都具有特定的功率要求。这对未来设备和处理管道的设计具有重要意义。
- **最新技术水平比较：**该数据集包含使用Zephyr Bioharness 3.0胸带测量的ECG信号的几个生理测量值。这使得能够使用来自不受头部/面部运动影响的商业设备的最先进的方法对应用于耳内数据的生命体征估计方法进行验证和基准测试。

虽然EarSet数据集为可穿戴设备开辟了新的机会，但我们的方法仍然存在一些限制，并为进一步改进提供了机会。我们的重点是提供一个数据集，以调查头/脸运动的影响，除了全身活动，在耳PPG信号质量和生命体征估计。肤色是可能影响数据质量的另一个因素。虽然EarSet提供了肤色的多样性，但所获得的数据在六种色素沉着类别中并不均匀分布。未来的工作将考虑扩大数据集，以包括更多的参与者，以统一覆盖所有肤色。

我们所有的参与者在数据收集时都很健康，没有心脏相关的疾病。

未来的数据收集工作将考虑具有可能影响PPG信号形态的潜在条件的参与者，即使不存在运动相关伪影。正确区分这两种情况将大大提高可穿戴设备的可信度，超越商业环境-有可能应用于临床环境。此外，该领域专家对PPG信号质量的手动评估将补充数据集，从而能够开发自动管道来估计专家级临床评估。

代码可用性

我们提供在数据收集过程中获得的原始数据文件，这些文件由用户标识符结构化。我们没有实现任何专门的代码来预处理数据。

投稿时间：2023年3月9日;受理时间：2023年11月17日;发表时间：xx xx xxxx December 2023

引用

1. Castaneda, D., Esparza, A., Ghamari, M., 索尔坦普尔角& Nazwald, H. 可穿戴光电容积脉搏波传感器及其在医疗保健领域的潜在应用。国际生物传感器和生物电子学杂志4, 195 (2018)。
2. 伊马纳加岛哈拉, H., 小柳S. & Tanaka, K.体积描记图二阶导数波形分量与动脉扩张性的相关性。日本心脏杂志39, 775-784 (1998)。
3. Suganthi湖, Manivannan, M., Kunwar, B. K., Joseph, G. & Danda, D.大动脉炎外周动脉信号的形态学分析。临床监测和计算杂志29, 87-95 (2015)。
4. 艾伦, J.光电体积描记法及其在临床生理测量中的应用。生理测量28, R1 (2007)。
5. Zhao, T. Trueheart: Continuous authentication on wrist-worn wearables using ppg-based biometrics.在IEEE INFOCOM 2020-IEEE计算机通信会议, 30-39 (IEEE, 2020)。
6. 李, B.-G., 荣格, S.-J.和Chung, W.-Y.实时生理和视觉监测车辆驾驶员的非侵入性困倦检测。IET通信5, 2461-2469 (2011)。

7. Ferlini, A. *et al.* In-ear ppg for vital signs. *IEEE Pervasive Computing* 1–10, <https://doi.org/10.1109/MPRV.2021.3121171> (2021).
8. Rupavatharam, S. & Gruteser, M. Towards in-ear inertial jaw clenching detection. In *Proceedings of the 1st International Workshop on Earable Computing*, 54–55 (2019).
9. Röddiger, T., Wolffram, D., Laubenstein, D., Budde, M. & Beigl, M. Towards respiration rate monitoring using an in-ear headphone inertial measurement unit. In *Proceedings of the 1st International Workshop on Earable Computing*, 48–53 (2019).
10. Truong, H., Montanari, A. & Kawsar, F. Non-invasive blood pressure monitoring with multi-modal in-ear sensing. In *ICASSP 2022-2022 IEEE International Conference on Acoustics, Speech and Signal Processing (ICASSP)*, 6–10 (IEEE, 2022).
11. Prakash, J., Yang, Z., Wei, Y.-L. & Choudhury, R. R. Stear: Robust step counting from earables. In *Proceedings of the 1st International Workshop on Earable Computing*, 36–41 (2019).
12. Ma, D., Ferlini, A. & Mascolo, C. Oesense: Employing occlusion effect for in-ear human sensing. In *Proceedings of the 19th Annual International Conference on Mobile Systems, Applications, and Services, MobiSys '21*, 175–187, <https://doi.org/10.1145/3458864.3467680> (Association for Computing Machinery, New York, NY, USA, 2021).
13. Kawsar, F., Min, C., Mathur, A. & Montanari, A. Earables for personal-scale behavior analytics. *IEEE Pervasive Computing* 17, 83–89 (2018).
14. Ferlini, A., Montanari, A., Mascolo, C. & Harle, R. Head motion tracking through in-ear wearables. In *Proceedings of the 1st International Workshop on Earable Computing*, 8–13 (2019).
15. Ferlini, A., Ma, D., Harle, R. & Mascolo, C. Eargate: gait-based user identification with in-ear microphones. In *Proceedings of the 27th Annual International Conference on Mobile Computing and Networking*, 337–349 (2021).
16. Ahuja, A., Ferlini, A. & Mascolo, C. PilotEar: Enabling In-Ear Inertial Navigation, 139–145 (Association for Computing Machinery, New York, NY, USA, 2021).
17. Ferlini, A., Ma, D., Qendro, L. & Mascolo, C. Mobile health with head-worn devices: Challenges and opportunities. *IEEE Pervasive Computing* (2022).
18. Choudhury, R. R. Earable computing: A new area to think about. In *Proceedings of the 22nd International Workshop on Mobile Computing Systems and Applications*, 147–153 (2021).
19. Nguyen, A. *et al.* A lightweight and inexpensive in-ear sensing system for automatic whole-night sleep stage monitoring. In *Proceedings of the 14th ACM Conference on Embedded Network Sensor Systems CD-ROM*, 230–244 (2016).
20. Hládek, L., Porr, B. & Brimijoin, W. O. Real-time estimation of horizontal gaze angle by saccade integration using in-ear electrooculography. *Plos one* 13, e0190420 (2018).
21. Bi, S. *et al.* Auracle: Detecting eating episodes with an ear-mounted sensor. *Proceedings of the ACM on Interactive, Mobile, Wearable and Ubiquitous Technologies* 2, 1–27 (2018).
22. Poh, M.-Z., Swenson, N. C. & Picard, R. W. Motion-tolerant magnetic earring sensor and wireless earpiece for wearable photoplethysmography. *IEEE Transactions on Information Technology in Biomedicine* 14, 786–794 (2010).
23. Passler, S., Müller, N. & Senner, V. In-ear pulse rate measurement: a valid alternative to heart rate derived from electrocardiography? *Sensors* 19, 3641 (2019).
24. Patterson, J. A., McIlwraith, D. C. & Yang, G.-Z. A flexible, low noise reflective ppg sensor platform for ear-worn heart rate monitoring. In *2009 sixth international workshop on wearable and implantable body sensor networks*, 286–291 (IEEE, 2009).
25. Venema, B., Schiefer, J., Blazek, V., Blanik, N. & Leonhardt, S. Evaluating innovative in-ear pulse oximetry for unobtrusive cardiovascular and pulmonary monitoring during sleep. *IEEE journal of translational engineering in health and medicine* 1, 270028–270028 (2013).
26. Kalanadhabhatta, M., Min, C., Montanari, A. & Kawsar, F. Fatiguset: A multi-modal dataset for modeling mental fatigue and fatigability (2021).
27. Zhang, Q., Zeng, X., Hu, W. & Zhou, D. A machine learning-empowered system for long-term motion-tolerant wearable monitoring of blood pressure and heart rate with ear-ecg/ppg. *IEEE Access* 5, 10547–10561, <https://doi.org/10.1109/ACCESS.2017.2707472> (2017).
28. Friesen, E. & Ekman, P. Facial action coding system: a technique for the measurement of facial movement. *Palo Alto* (1978).
29. Fitzpatrick, T. B. The validity and practicality of sun-reactive skin types i through vi. *Archives of dermatology* 124, 869–871 (1988).
30. Kim, J.-H., Roberge, R., Powell, J., Shafer, A. & Williams, W. J. Measurement accuracy of heart rate and respiratory rate during graded exercise and sustained exercise in the heat using the zephyr bioharnesstm. *International journal of sports medicine* 497–501 (2012).
31. Tailor, S. A., Chauhan, J. & Mascolo, C. A first step towards on-device monitoring of body sounds in the wild. In *Adjunct Proceedings of the 2020 ACM International Joint Conference on Pervasive and Ubiquitous Computing and Proceedings of the 2020 ACM International Symposium on Wearable Computers*, 708–712 (2020).
32. Lee, S. *et al.* Automatic smile and frown recognition with kinetic earables. In *Proceedings of the 10th Augmented Human International Conference 2019, AH2019*, <https://doi.org/10.1145/3311823.3311869> (Association for Computing Machinery, New York, NY, USA, 2019).
33. Verma, D., Bhalla, S., Sahnani, D., Shukla, J. & Parnami, A. Expressesar: Sensing fine-grained facial expressions with earables. *Proceedings of the ACM on Interactive, Mobile, Wearable and Ubiquitous Technologies* 5, 1–28 (2021).
34. Choi, S. *et al.* Ppgface: Like what you are watching? earphones can “feel” your facial expressions. *Proceedings of the ACM on Interactive, Mobile, Wearable and Ubiquitous Technologies* 6, 1–32 (2022).
35. Bent, B., Goldstein, B. A., Kibbe, W. A. & Dunn, J. P. Investigating sources of inaccuracy in wearable optical heart rate sensors. *NPJ digital medicine* 3, 1–9 (2020).
36. Association, C. T. *et al.* Ansi/cta standard. physical activity monitoring for heart rate. Tech. Rep., ANSI/CTA-2065 (2018).
37. Dehkordi, P., Garde, A., Molavi, B., Ansermino, J. M. & Dumont, G. A. Extracting instantaneous respiratory rate from multiple photoplethysmogram respiratory-induced variations. *Frontiers in Physiology* 9, <https://doi.org/10.3389/fphys.2018.00948> (2018).
38. Shuzan, M. N. I. *et al.* A novel non-invasive estimation of respiration rate from photoplethysmograph signal using machine learning model 2102.09483 (2021).
39. Tazarv, A. & Levorato, M. A deep learning approach to predict blood pressure from ppg signals 2108.00099 (2021).
40. cao, y., Chen, H., Li, F. & Wang, Y. Crisp-bp: Continuous wrist ppg-based blood pressure measurement. <https://doi.org/10.1145/3447993.3483241> (2022).
41. Perpetuini, D. *et al.* Multi-site photoplethysmographic and electrocardiographic system for arterial stiffness and cardiovascular status assessment. *Sensors* 19, 5570 (2019).
42. Orphanidou, C. Signal quality assessment in physiological monitoring: state of the art and practical considerations. (2017).
43. Ferlini, A., Montanari, A., Balaji, A. N., Mascolo, C. & Kawsar, F. EarSet: A Multi-Modal In-Ear Dataset. *Zenodo* <https://doi.org/10.5281/zenodo.8142332> (2023).
44. Biagetti, G. *et al.* Dataset from ppg wireless sensor for activity monitoring. *Data in Brief* 29, 105044, <https://doi.org/10.1016/j.dib.2019.105044> (2020).
45. Reiss, A., Indlekofer, I., Schmidt, P. & Van Laerhoven, K. Deep ppg: Large-scale heart rate estimation with convolutional neural networks. *Sensors* 19, <https://doi.org/10.3390/s19143079> (2019).
46. Jarchi, D. & Casson, A. J. Description of a database containing wrist ppg signals recorded during physical exercise with both accelerometer and gyroscope measures of motion. *Data* 2, <https://doi.org/10.3390/data2010001> (2017).
47. Tan, C. W., Bergmeir, C., Petitjean, F. & Webb, G. I. Ieeppg dataset. *Zenodo* <https://doi.org/10.5281/zenodo.3902710> (2020).

7. Ferlini, A.等人, In-ear ppg for vital signs. IEEE普适计算1 <https://doi.org/10.1109/MPRV.2021.3121171>
8. Rupavatharam, S. & Gruteser, M.面向耳内惯性咬颤检测。在第一届可穿戴计算国际研讨会论文集, 54-55 (2019)。
9. Röddiger, T., Wolfram, D., Laubenstein, D., Budde, M. & Beigl, M.使用入耳式耳机惯性测量单元进行呼吸率监测。在第一届可穿戴计算国际研讨会论文集, 48-53 (2019)。
10. Truong, H., Montanari, A. & Kawsar, F.具有多模态耳内感知的非侵入式血压监测。在ICASSP 20222022 IEEE声学, 语音和信号处理国际会议 (ICASSP) , 6-10 (IEEE, 2022)。
11. Prakash, J., 杨志, 魏, Y.-L. & Choudhury, R. R. Stear: 来自耳听设备的强大步数计数。在第一届可穿戴计算国际研讨会论文集, 36-41 (2019)。
12. 妈妈, D., Ferlini, A. & Mascolo, C. Oesense: 采用遮挡效应进行耳内人体感知。In Proceedings of the 19 th Annual International Conference on mobileSystems, Applications, and Services, 《移动系统》21, 175-187, <https://doi.org/10.1145/3458864.3467680> (美国纽约州纽约计算机协会, 2021年)。
13. Kawsar, F., Min, C., 马图尔A. & Montanari, A.用于个人规模行为分析的可穿戴设备。IEEE普适计算17, 83-89 (2018)。
14. Ferlini, A., Montanari, A., 马斯科洛角& Harle, R.通过入耳式可穿戴设备进行头部运动跟踪。在第一届可穿戴计算国际研讨会论文集, 8-13 (2019)。
15. Ferlini, A., 妈妈, D., 哈尔河& Mascolo, C.耳门: 使用入耳式麦克风进行基于步态的用户识别。在第27届移动的计算和网络年度国际会议论文集, 337-349 (2021)。
16. Ahuja, A., Ferlini, A. & Mascolo, C. PilotEar: 启用耳内惯性导航, 139 - 145 (计算机协会, 纽约, 纽约, 美国, 2021年)。
17. Ferlini, A., 妈妈, D., 肯德罗湖& Mascolo, C.头戴式设备的移动的健康: 挑战和机遇。IEEE普适计算 (2022)。
18. 乔杜里河, 巴西-地R.可穿戴计算: 一个值得思考的新领域第22届移动的计算系统和应用国际研讨论文集, 147 - 153 (2021)。
19. 阮氏A. A lightweight and economic inear sensing system for automatic whole-night sleep stage monitoring. 第14届ACM嵌入式网络传感器系统会议论文集CD-ROM, 230 - 244 (2016)。
20. Hladek湖, 波尔, B. & Brimijoin, W.O.利用耳内眼电图以扫视整合即时估测水平凝视角度。Plos one 13, e0190420 (2018)。
21. Bi, S. Auracle: Detecting eating episodes with an ear-mounted sensor. Proceedings of the ACM on Interactive, 移动的, Wearable and Ubiquitous Technologies 2, 1-27 (2018)。
22. Poh, M. Z., Swenson, N. C. & Picard, R. W.可穿戴式光电容积脉搏波仪的运动容限磁性耳环传感器和无线耳机。IEEE Transactions on Information Technology in Biomedicine 14, 786-794 (2010)。
23. Passler, S., Müller, N.耳内脉搏率测量: 心电图心率的有效替代方法? 传感器19, 3641 (2019)。
24. 帕特森, J.A., McIlwraith, D.C. & Yang, G.-Z.用于耳戴式心率监测的灵活、低噪声反射式PPG传感器平台。2009年第六届可穿戴和植入式身体传感器网络国际研讨会, 286-291 (IEEE, 2009)。
25. Venema, B., Schiefer, J., Blazek, V., Blanik, N. & Leonhardt, S.评估创新的入耳式脉搏血氧仪在睡眠期间用于非侵入性心血管和肺监测。IEEE Journal of Translational Engineering in Health and Medicine 1, 2700208-2700208 (2013)。
26. Kalanadhabhatta, M., Min, C., Montanari, A. & Kawsar, F.《精神疲劳和疲劳建模的多模态数据集》 (2021)。
27. 张, Q., 曾光, 胡, W. & Zhou, D.一个机器学习授权的系统, 用于通过耳式心电图/ppg进行长期运动耐受的血压和心率可穿戴监测。IEEE Access 5, 10547 <https://doi.org/10.1109/ACCESS.2017.2707472>
28. 弗里森, E. Ekman, P. Facial action coding system: a technique for the measurement of facial movement. Palo Alto (1978)。
29. 菲茨帕特里克, T. B. 太阳反应性皮肤类型的有效性和实用性。Archives of dermatology 124, 869-871 (1988)。
30. 金, J. - H. & 罗贝河, 鲍威尔, J., Shafer, A. & 威廉姆斯, W.J.使用Zephyr bioharnesstm测量分级运动和高温持续运动期间心率和呼吸率的准确性。国际运动医学杂志497-501 (2012)。
31. Tailor, S.-, Chauhan, J. & Mascolo, C.这是在设备上监测野外身体声音的第一步。在2020年ACM普适和普适计算国际联合会议的附属会议录和2020年ACM可穿戴计算机国际研讨会的会议录, 708-712 (2020)。
32. 李, S. 使用动态耳片进行自动微笑和皱眉识别。在2019年第10届增强人类国际会议论文集, AH 2019, <https://doi.org/10.1145/3311823.3311869> (计算机协会, 纽约, 纽约, 美国, 2019)。
33. Verma, D., Bhalla, S., Sahnan, D., Shukla, J. & Parnami, A. Expresssear: 用耳听设备感知精细的面部表情。ACM关于交互式, 移动的, 可穿戴和无处不在的技术的会议记录5, 1-28 (2021)。
34. 崔, S. Ppgface: 喜欢你正在看的吗? 耳机可以“感觉”你的面部表情。ACM关于交互式, 移动的, 可穿戴和无处不在的技术的会议记录6, 1-32 (2022)。
35. 本特, B., 戈尔茨坦, B. 一、Kibbe, W. A. & Dunn, J. P. Investigating sources of inaccuracy in wearable optical heart rate sensors. NPJ数字医学3, 1-9 (2020)。
36. 协会角T.等人, Ansi/cta标准。监测心率的身体活动。Tech.代表: ANSI/CTA-2065 (2018)。
37. Dehkordi, P., Garde, A., Molavi, B., Ansermino, J. M. & Dumont, G. A.从多次光电容积脉搏波诱发的变化中提取瞬时呼吸频率。Frontiers in Physiology 9, <https://doi.org/10.3389/fphys.2018.00948> (2018)。
38. Shuzan, M. N. I.等人, 使用机器学习模型2102.09483 (2021) 从光电体积描记器信号对呼吸率进行新的非侵入性估计。
39. Tazarv, A. & Levorato, M.从ppg信号预测血压的深度学习方法2108.00099 (2021)。
40. Cao, Y., 陈洪, Li, F.和Wang, Y. Crisp-BP: 基于腕部PPG的连续血压测量。网址: <https://doi.org/10.1145/3447993.3483241> (2022)。
41. Perpetuini, D.等人, 用于动脉僵硬度和心血管状态评估的多部位光电体积描记和心电图系统。传感器19, 5570 (2019)。
42. 奥法尼杜角生理监测中的信号质量评估: 最新技术水平和实际考虑。 (2017年)。
43. Ferlini, A., Montanari, A., Balaji, A. N., 马斯科洛角& Kawsar, F. EarSet: 多模态耳内数据集。Zenodo <https://doi.org/10.5281/zenodo.8142332> (2023)。
44. Biagetti, G.来自PPG无线传感器的活动监测数据集。Data in Brief 29, 105044, <https://doi.org/10.1016/j.dib.2019.105044> (2020)。
45. Reiss, A., 因德勒克夫岛, 施密特, P.&货车Laerhoven, K. Deep ppg: 使用卷积神经网络进行大规模心率估计。Sensors 19, <https://doi.org/10.3390/s19143079> (2019)。
46. Jarchi, D. & Casson, A. J.包含在体育锻炼期间利用加速度计和陀螺仪运动测量记录的手腕ppg信号的数据库的描述。Data 2, <https://doi.org/10.3390/data2010001> (2017)。
47. 坦角, 澳-地W., Bergmeir, C., Petitjean, F. & Webb, G. I. Ieepg数据集。Zenodo <https://doi.org/10.5281/zenodo.3902710> (2020)。

48. Lee, H., Chung, H. & Lee, J. Motion artifact cancellation in wearable photoplethysmography using gyroscope. *IEEE Sensors Journal* **19**, 1166–1175, <https://doi.org/10.1109/ISEN.2018.2879970> (2019).
49. Schmidt, P., Reiss, A., Duerichen, R., Marberger, C. & Van Laerhoven, K. Introducing wesad, a multimodal dataset for wearable stress and affect detection. In *Proceedings of the 20th ACM International Conference on Multimodal Interaction*, ICMI '18, 400–408, <https://doi.org/10.1145/3242969.3242985> (Association for Computing Machinery, New York, NY, USA, 2018).
50. Pimentel, M. A. F. *et al.* Toward a robust estimation of respiratory rate from pulse oximeters. *IEEE Transactions on Biomedical Engineering* **64**, 1914–1923, <https://doi.org/10.1109/TBME.2016.2613124> (2017).
51. Rocha, L. G. *et al.* Real-time hr estimation from wrist ppg using binary lstms. In *2019 IEEE Biomedical Circuits and Systems Conference (BioCAS)*, 1–4 (IEEE, 2019).
52. Jarchi, D. *et al.* Estimation of hrv and spo2 from wrist-worn commercial sensors for clinical settings. In *2018 IEEE 15th International Conference on Wearable and Implantable Body Sensor Networks (BSN)*, 144–147 (IEEE, 2018).
53. Lu, S. *et al.* Can photoplethysmography variability serve as an alternative approach to obtain heart rate variability information? *Journal of clinical monitoring and computing* **22**, 23–29 (2008).
54. Hoog Antink, C. *et al.* Accuracy of heart rate variability estimated with reflective wrist-ppg in elderly vascular patients. *Scientific reports* **11**, 1–12 (2021).
55. Chang, H.-H. *et al.* A method for respiration rate detection in wrist ppg signal using holo-hilbert spectrum. *IEEE Sensors Journal* **18**, 7560–7569 (2018).
56. Dubey, H., Constant, N. & Mankodiya, K. Respire: A spectral kurtosis-based method to extract respiration rate from wearable ppg signals. In *2017 IEEE/ACM International Conference on Connected Health: Applications, Systems and Engineering Technologies (CHASE)*, 84–89 (IEEE, 2017).
57. Behar, J. *et al.* Sleepap: an automated obstructive sleep apnoea screening application for smartphones. *IEEE journal of biomedical and health informatics* **19**, 325–331 (2014).
58. Korkalainen, H. *et al.* Deep learning enables sleep staging from photoplethysmogram for patients with suspected sleep apnea. *Sleep* **43**, zsaa098 (2020).
59. Bonomi, A. G. *et al.* Atrial fibrillation detection using photo-plethysmography and acceleration data at the wrist. In *2016 computing in cardiology conference (cinc)*, 277–280 (IEEE, 2016).
60. Nemati, S. *et al.* Monitoring and detecting atrial fibrillation using wearable technology. In *2016 38th Annual International Conference of the IEEE Engineering in Medicine and Biology Society (EMBC)*, 3394–3397 (IEEE, 2016).
61. Miao, F., Wang, X., Yin, L. & Li, Y. A wearable sensor for arterial stiffness monitoring based on machine learning algorithms. *IEEE Sensors Journal* **19**, 1426–1434 (2018).
62. Falter, M. *et al.* Accuracy of apple watch measurements for heart rate and energy expenditure in patients with cardiovascular disease: Cross-sectional study. *JMIR mHealth and uHealth* **7**, e11889 (2019).
63. Balaji, A. N., Yuan, C., Wang, B., Peh, L.-S. & Shao, H. ph watch-leveraging pulse oximeters in existing wearables for reusable, real-time monitoring of ph in sweat. In *Proceedings of the 17th Annual International Conference on Mobile Systems, Applications, and Services*, 262–274 (2019).
64. Posada-Quintero, H. F. *et al.* Mild dehydration identification using machine learning to assess autonomic responses to cognitive stress. *Nutrients* **12**, 42 (2020).
65. Facs – facial action coding system. <https://imotions.com/blog/learning/research-fundamentals/facial-action-coding-system/> Last Accessed: 2023-03-08.

Author contributions

All authors participated in the design of the study protocol. A.F., A.N.B and A.M. conducted the experiments. F.K., A.M and C.M. supervised the project. A.F. prepared a first draft of the manuscript. All authors edited, revised, and approved the final version of the manuscript.

Competing interests

The authors declare no competing interests.

Additional information

Correspondence and requests for materials should be addressed to A.M. or A.F.

Reprints and permissions information is available at www.nature.com/reprints.

Publisher's note Springer Nature remains neutral with regard to jurisdictional claims in published maps and institutional affiliations.



Open Access This article is licensed under a Creative Commons Attribution 4.0 International License, which permits use, sharing, adaptation, distribution and reproduction in any medium or format, as long as you give appropriate credit to the original author(s) and the source, provide a link to the Creative Commons licence, and indicate if changes were made. The images or other third party material in this article are included in the article's Creative Commons licence, unless indicated otherwise in a credit line to the material. If material is not included in the article's Creative Commons licence and your intended use is not permitted by statutory regulation or exceeds the permitted use, you will need to obtain permission directly from the copyright holder. To view a copy of this licence, visit <http://creativecommons.org/licenses/by/4.0/>.

© The Author(s) 2023

48. 李， H。 Chung， H。 作者： J. Motion Article Cancellation in Wearable photoplethysmography， Using Gyroscope . IEEE Sensors Journal 19 , 1166 - 1175 , <https://doi.org/10.1109/JSEN.2018.2879970> (2019) 。
49. 史密斯， P. Reiss， A. 杜特尔特， R. 马尔堡， C. Van Laerhoven， K. 介绍 Wesad ，一种用于可穿戴压力和影响检测的多模式数据集。第 20 届 ACM 国际多模态交互会议 (ICMI '18 , 400 - 408) <https://doi.org/10.1145/3242969.3242985> (Association for Computing Machinery , New York , NY , USA , 2018) 。
50. 皮卡丘， M. A. A. F 研究人员对呼吸率与脉搏氧饱和度进行了有力的估计。 IEEE Transactions on Biomedical Engineering 64 , 1914 - 1923 , 1914 年 <https://doi.org/10.1109/TBME.2016.2613124> (2017) 。
51. 罗克， L. g. et al. Real-time hr estimation from wrist ppg using binary lstms . 使用二进制 Lstms 。 2019 年 IEEE 生物医学电路和系统会议 (BioCAS) , 1 - 4 (IEEE , 2019) 。
52. Jarchi, D. 等人, Estimation of hrv and spo 2 from wrist-worn commercial sensors for clinical settings. 2018 年 IEEE 第 15 届可穿戴和植入式身体传感器网络国际会议 (BSN) , 144-147 (IEEE , 2018) 。
53. Lu, S. 光电容积描记术变异性能否作为获得心率变异性信息的替代方法? Journal of Clinical Monitoring and Computing 22 , 23-29 (2008) 。
54. Hoog Antink, C. 等人, 老年血管患者中使用反射性腕部 ppg 估计的心率变异性准确性。科学报告 11 , 1-12 (2021) 。
55. 张, H.- H. 等人, A method for respiratory rate detection in wrist ppg signal using holo-hilbert spectrum. IEEE Sensors Journal 18 , 7560-7569 (2018) 。
56. Dubey, H., Constant, N. & Mankodiya, K. Respi: 一种基于谱峰的方法, 用于从可穿戴 ppg 信号中提取呼吸率。 2017 年 IEEE/ACM 互联健康国际会议: 应用, 系统和工程技术 (CHASE) , 84-89 (IEEE , 2017) 。
57. Behar, J. et al. Sleepap: an automated obstructive sleep apnoea screening application for smartphones. IEEE Journal of Biomedical and Health Informatics 19 , 325-331 (2014) 。
58. Korkalaainen, H. Deep learning enables sleep staging from photoplethysmogram for patients with suspected sleep apnea. 深度学习使疑似睡眠呼吸暂停患者能够从光电容积描记图进行睡眠分期。睡眠 43 , zsaa 098 (2020) 。
59. Bonomi, A. G. 等人, Atrial fibrillation detection using photo-plethysmography and acceleration data at the wrist. 在 2016 年心脏病学计算会议 (cinc) , 277-280 (IEEE , 2016) 。
60. Nemati, S. 使用可穿戴技术监测和检测心房颤动。 2016 年第 38 届 IEEE 医学和生物学工程学会 (EMBC) 国际年会, 3394-3397 (IEEE , 2016) 。
61. Miao, F., 王, X., 因湖, 澳-地和李, Y. 基于机器学习算法的动脉硬度监测可穿戴传感器。 IEEE Sensors Journal 19 , 1426-1434 (2018) 。
62. 法特尔, M. Apple Watch 测量心血管疾病患者心率和能量消耗的准确性: 横断面研究。 JMIR mHealth 和 uHealth 7 , e11889 (2019) 。
63. Balaji, A. N., 袁角, 越-地 Wang, B., 佩湖 S. & Shao, H. pH 值监测-利用现有可穿戴设备中的脉搏血氧仪, 用于可重复使用的实时监测汗液中的 pH 值。第 17 届移动的系统、应用和服务国际年会论文集, 262-274 (2019) 。
64. Posada-Quintero, H. F. 使用机器学习评估对认知压力的自主反应的轻度脱水识别。营养素 12 , 42 (2020) 。
65. 面部表情编码系统. <https://imotions.com/blog/learning/research-fundamentals/facial-action-coding-system/> 最后访问时间: 2023-03-08.

作者贡献

所有作者均参与了研究方案的设计。 A.F. , A.N.B 和 A.M. 进行了实验。 F.K. , 上午和下午。 监督这个项目。 A.F. 准备了手稿的初稿。 所有作者编辑、修订并批准了手稿的最终版本。

相互竞争的利益

作者声明没有竞争利益。

附加信息

信件和索取材料的要求应寄往 A.M. 或 A.F. 。

转载和许可信息可在 www.nature.com/reprints 上获得。

出版商的说明 Springer Nature 在已出版地图和机构附属关系中的管辖权主张方面保持中立。

 根据知识共享署名 4.0 国际许可协议授权, 该协议允许以任何媒介或格式使用、共享、改编、分发和复制, 只要您给予适当的署名给原作者和来源, 提供知识共享许可协议的链接, 并注明是否进行了更改。本文中的图片或其他第三方材料包含在文章的知识共享许可证中, 除非在材料的信用额度中另有说明。如果材料未包含在文章的知识共享许可中, 并且您的预期用途不受法律法规的允许或超出了允许的用途, 则您需要直接从版权保持器获得许可。要查看本许可证的副本, 请访问 <http://creativecommons.org/licenses/by/4.0/> 。

© 作者 2023